4E analysis and three-objective optimization for selection of the best prime mover in smart energy systems for residential applications: a comparison of four different scenarios

Ehsan Gholamian[1] [iD] · Pedram Hanafizadeh[1] · Pouria Ahmadi[1] · Livio Mazzarella[2]

Abstract

Recently, using integrated energy systems for residential-scale applications has been of great interest to the researchers. The objective of this study is the proposal, techno-economic analysis, and optimization of the best prime mover for the residential scale combined cooling, heating, and power generation system (CCHP). Different prime movers consisting of solid oxide fuel cell (SOFC), internal combustion engine (ICE), microgas turbine (MGT), and hybrid SOFC/GT system for power production are integrated with HRSG and double effect Li/Br refrigeration system for heating and cooling generation, respectively. A parametric study is conducted on the best case to find the key decision variables. Also, a very cutting-edge optimization, which is 3D multi-objective optimization, is carried out for minimizing the unit product cost and emission and maximizing the exergetic efficiency. Results revealed that the hybrid SOFC/GT has higher exergy efficiency of 69.06% and unit product cost of 37.78 \$ GJ^{-1}, among other case studies. Also, optimization results indicate a maximum exergy efficiency of 73.15%, and a minimum cost of 25.08 (\$ GJ^{-1}) can be reached for the SOFC-/GT-based CCHP system. Moreover, the optimized emission for the best-case scenario becomes 62.52 g MWh^{-1}.

List of symbols

A	Area, m^2
c	Specific exergy cost, \$ GJ^{-1}
$\dot{C}$	Cost rate, \$ h^{-1}
$\dot{E}$	Exergy rate, kW
f	Exergoeconomic factor
F	Faraday constant, C mol^{-1}
$\Delta\bar{g}^0$	Change in molar Gibbs free energy, J/mol
h	Enthalpy
i_r	Interest rate
j	Current density, A m^{-2}
J	PEME current density
K	Equilibrium constant
LHV_f	Fuel lower heating value
M	Molar mass
$\dot{m}_f$	Fuel mass flow rate
N	Operating hours, h
$n_1, n_2, \ldots, n_7$	Mole number of reaction components
n_e	Number of electrons produced per hydrogen mole
$\dot{n}$	Molar flow rate
N_C	Number of cells in the stack
P	Pressure
PR	Pressure ratio
p_{H_2O}	Partial pressure of H$_2$O
p_{H_2}	Partial pressure of H$_2$
p_{O_2}	Partial pressure of O$_2$
$\dot{Q}_{high}$	Heat rate of the heater inside the Stirling engine, kW
$\dot{Q}_{loss}$	Heat loss rate of cooler inside the Stirling engine, kW
R	Total ohmic resistance
R_{AR}	Anode recycling ratio
R_{CR}	Cathode recycling ratio

✉ Pedram Hanafizadeh
hanafizadeh@ut.ac.ir

✉ Pouria Ahmadi
Pahmadi@ut.ac.ir

1   Centre of Excellence in Design and Optimization, School of Mechanical Engineering, University of Tehran, Tehran, Iran

2   Department of Energy, Polytechnic University of Milan, Milan, Italy

$\bar{R}$	Universal gas constant, J mol^{-1} K
RV	Piston compression ratio of Stirling engine
s	Specific entropy
T	Temperature
T_g	Gasification temperature
U_f	Fuel utilization ratio
V	Voltage, V
V_0	Reversible potential
V_C	Cell voltage, V
V_{loss}	Loss voltage, V
V_N	Reversible cell voltage, V
w	Mole fraction of moisture in the biomass (kmol/kmol)
$\dot{W}$	Power, kW
y_i	Molar fraction
y_r	Extent of water gas shift reaction, mol/s
x_r	Extent of steam reforming reaction for methane, mol/s
$\dot{Z}$	Cost rate of components, $ h^{-1}
$\dot{Z}^{CI}$	Capital investment cost rate of components, $ h^{-1}
$\dot{Z}^{OM}$	Operating and maintenance cost rate of components, $ h^{-1}

Superscripts

ch	Chemical
ph	Physical

Subscripts and abbreviations

0	Dead state
act	Activation
AB	Afterburner
AC	Air blower
an	Anode
AHX	Air heat exchanger
ca	Cathode
CEPI	Chemical Engineering Plant Cost Index
conc	Concentration
CRF	Capital recovery factor
D	Destruction
e	Electrolyte
FC	Fuel blower
FHX	Fuel heat exchanger
HS, gas	Highest Stirling gas temperature
i	Inlet
INV	DC to AC inverter
k	kth component
L	Loss
LS, gas	Lowest Stirling gas temperature
MC	Moisture content
PM	Prime mover
GT	Gas turbine
CCHP	Combined cooling heating and power

CHP	Combined heating and power
ICE	Internal combustion engine
PY	Present year
R	Reforming
S	Shifting
SOFC	Solid oxide fuel cell
SE	Stirling engine
tot	Total

Greek letters

η_{pcy}	Polytrophic efficiency
$\eta_{mech, SE}$	Stirling mechanical efficiency
ε	Emission indicator
ε_{SE}	Heater efficiency inside the Stirling engine
ζ	Lowest to highest temperature of Stirling engine
γ	Ratio of specific heats
η_I	Energy efficiency
η_{II}	Exergy efficiency
φ	Maintenance factor
τ	Annual plant operation hours
σ	Total ionic conductivity
λ	Content of water

Introduction

A combined cooling, heating, and power generation system shows higher capability in energy and cost-saving, as well as its flexibility and reliability in generating power, and thus becomes one of the most promising methods of energy conversion [1]. Also, the total efficiency of thermal power plants in Iran and in general is between 30 and 50% while considering 20% transmission losses; the distributed energy generation seems more perspective [2].

One of the main concerns of designing the CCHP system for residential applications is the selection of high-efficiency prime movers. Different models of integration of the CCHP system have been studied with different prime movers in the literature [3, 4], as many of them either studied single PMs in energetic or economic points of view. In this regard, Kaldehi et al. [5] studied a micro-Stirling engine as a prime mover of a CCHP system in the residential sector for different climates. They found out that the integration of the Stirling engine with heating and cooling cycles results in a significant amount of emission reduction. Their results revealed that maximum CO_2 reduction in every climate is more than 40%. Also, Mojaver et al. [6] investigated an SOFC-based power generation system and found out that at optimum conditions, the efficiency and emission are 48.03% and 281.4 kg/MW.h, respectively. Abbasi et al. [7] studied ICE and GT as prime movers of a CCHP and considered the economic and exergetic factors of the system. They found out that energy

efficiency will increase up to 10% if both prime movers are selected in one order. Also, the best scenario was combining the ICE and GT as prime movers and 87% energy efficiency, 62.8% exergy efficiency, and operating cost reduction of about 80% are obtained. Optimal design and operation strategy for integrated evaluation of CCHP (combined cooling heating and power) system is studied by Cai et al. [8]. Mehrpouya et al. [9] studied technical performance analysis of a (CCHP) system based on (SOFC) technology for educational building applications. The SOFC efficiency of 120 kW was about 45% while the hybrid system electrical cooling efficiency reached 58%, and the total CCHP system was 60% efficient. Also, they found out that the capital recovery factor is 8.3 years. Moreover, using SOFC and gas turbines as prime movers of CCHP systems has been of great interest to the researchers. Wang et al. [10] investigated the CCHP system integrating gas turbine and heat-driven cooling/power cogeneration. The main result of their research was that the CCHP system could consume 31% less natural gas than stand-alone power generation systems. Optimization and analysis of the CCHP system based on energy load coupling of residential and office buildings were carried out by Li et al. [11]. They found out that increasing gas prices will result in increased air-conditioning cooling load. Also, using SOFC-based CCHP system in residential buildings in China is studied by Jing et al. [12]. Their study included a comparison between SOFC-based CCHP and combustion-based ones, which resulted in that SOFC-CCHP systems demonstrate outstanding performance on energy efficiency as well as reducing carbon emission. Abbasi et al. [13] proposed a methodology to size the CCHP systems prime movers for large-scale residential buildings. Their results show that ICE-based trigeneration system is beneficial in all climates of the study. But the more important finding was that determining the right CCHP system is a far better solution for every environment. Many researchers have put their best effort in gas turbine and fuel cell analysis and optimization [14, 15]. Farahnak et al. [16] used ICE as the prime mover of the CCHP system and found out that using the CCHP system in small buildings results in 17.24% energy saving, but in large buildings, it causes 5.1% energy saving. Also, according to their study, the optimal payback period for large residential buildings is found to be 5.08 years. Feng et al. studied the performance analysis of a CCHP system with different cooling supply modes [17]. Moghimi et al. [18] studied GT-based CCHP systems, and a 4E analysis is performed to show that the CCHP system has 7% higher exergy efficiency and 12% higher energy efficiency instead than stand-alone Brayton cycle. Exergy analysis is identified as a very powerful and cutting-edge tool in analyzing the power plants, which helps the scientists define the inefficiencies in the systems and improve the effectiveness of these power plants [9, 19]. In this regard, Ansarinasab et al. [20] developed an exergy-based investigation (exergy,

exergoeconomic, etc.) of hydrogen liquefaction plant. Moreover, in a review study, Ahmadi et al. [21], investigated the thermodynamic and economic analysis of performance evaluation of all the thermal power plants and they found out that exergy analysis enables designers to make intricate thermodynamic systems operate more efficiently. Al Moussavi et al. [22] studied optimal management of SOFC-based CCHP systems for residential applications. Two strategies for the operation were employed: off-grid following electrical load and on-grid baseload operations. Their optimized results show that the CCHP system performs better from energetic and economic points of view. The maximum energy and exergy efficiencies (65.2% and 45.77%) and minimum system cost rate (22.2 cents kWh^{-1}) are obtained under on-grid baseload operation for the CCHP system. Yousefi et al. [23] studied the component sizing of a hybrid ICE + PV/T-driven CCHP microgrid system and optimized the system multi-objectively. The results discovered that, regardless of slight growth in the average rate of net present cost, the combined cooling, heating, and power system integrated with solar energy has a substantially better performance in energy saving and emissions than the ICE-driven system. Rey et al. [24] analyzed the performance of an ICE-based CCHP and compared it with experimental data. Results revealed that maximum electrical efficiency is 7.63%, and it is obtained when the heat pump is off, and the engine is operating at a low speed. Also, they reported that the higher performance of the gas engine-driven heat pump is 10.79% when the engine is running at high speed. Luo et al. [25] studied a multisupply multidemand control strategy for combined cooling, heating, and power system primed with SOFC and gas turbine. Also, Chen et al. [26] investigated the Multi-criteria assessment and optimization study on a 5 kW PEMFC-based residential CCHP system. The optimized results show that exergy efficiency, cost, and GHG emission are 39.9%, 29337.3$, and 1.8×10^7 gr, respectively, at optimal points. Chitgar et al. [27] proposed an integrated energy system based on SOFC. The optimization results in their works showed that an optimal point exergy efficiency and total cost rate are 54% and 36.8 $ h^{-1}, respectively. Behzadi et al. [28] studied a hybrid renewable system and found out that in case of considering cooling set for absorption chiller, it has the highest exergy destruction rate. Jokar et al. [29] carried out a multi-objective optimization of hybrid fuel cell systems and figured out that in optimum case the exergy destruction becomes 1.314 and rate density meets 0.3864 kW m^{-2}. Safari and Dincer [30] developed a novel biomass fired multigeneration system with hydrogen production. They found out that the energy and exergy efficiency of hybrid system reaches 40% and 63.6%, respectively. Beigzadeh et al. [31] modeled a SOFC and absorption chiller using nanofluids as heat transporters. They found out that nanofluid would result in an improve about 6&in efficiency.

There is a growing attention to the importance of prime movers of CCHP systems to reach maximum efficiency and the techno-economic and environmental analysis of these systems. However, little work is done on the comprehensive analysis and a complete multi-objective optimization of 3 counterparts of the simulation. To summarize the literature survey from the perspective of the present study, the research background is gathered in Table 1, which indicates the authors' motivations to carry out the study.

Some latest research on economic and environmental analysis of building-integrated CCHP systems reveals the importance of techno-economic and environmental analysis of these systems.

In this paper, the trigeneration system is proposed to supply the heating and cooling, along with the power demand in a residential building. A comparison is made to find the best prime mover for the CCHP system between SOFC, GT, and ICE, considering the efficiency, emission, and economic factors. The parametric study of key design variables like (stack temperature difference, fuel utilization factor, compressor pressure ratio and pinch point temperature difference, etc.) defines the domain of optimization. The scenario analysis helps us select the best prime mover based on the needs of the building, for example, power, heating, or cooling. Also, each study in the literature has focused on certain area and objective like optimizing energy, exergy, cost, or emission. Considering the literature survey (as illustrated in Table 1), there is a knowledge gap of a comprehensive analysis of the optimized prime mover's selection in microsize following main objectives and novelties as below:

- Comprehensive exergy, exergoeconomic, and environmental analysis of four CCHP systems and multi-objective optimization of the best prime mover case.
- Considering the low price of fuel for Tehran (instead of biomass or solar power), to result in an excellent payback period.
- Evolutionary-based, 3-dimensional multi-objective optimization of the best-case scenario, to find the higher exergetic efficiency and lower emission and unit product cost.
- Using a hybrid renewable energy system with considering heat recovery options for HRSG and refrigeration system.
- Comparison of SOFC, ICE, and MGT for residential application power production

System description and assumptions

Figure 1 shows the schematic diagram of the different scenarios proposed in this study. The prime mover of the CCHP system for power production might be stand-alone, SOFC (scenario 1), ICE (scenario 2), MGT (scenario 3), or hybrid SOFC-GT (scenario 4). The systems are considered in a way

that the power generation is different in 4 scenarios, and the exiting streams play the same role in the generation of heating and cooling. The exciting high-temperature combustion products are used in a heat recovery system to produce hot water for domestic use and in a double effect Li/Br system for production of refrigeration, respectively. In the first case, a fuel cell is considered for power generation, and HRSG and chiller are used to generate heating and cooling, respectively. The fuel is blown into the fuel mixer in state 7. In the fuel mixer, it is mixed up with the return stream from the fuel cell at 8b and exits to go through the fuel cell at state 8. On the other hand, the air is brought to the cathode to be reacted with fuel after being mixed in the mixer and passed through an air heat exchanger to raise the fluid temperature to the temperature of the cathode. After electrochemical reaction occurs in the fuel cell stack, the exiting streams mix and burn in the afterburner to ensure there is not any unreacted gas to be wasted and raise the temperature to higher levels. The existing gas at state 10 heats the air at AHX and then goes through the HRSG and double effect lithium bromide cycle to produce hot water and cooling. If the hot gases are warm enough, it will pass through a single turbine (scenario 4) to provide extra power. The description of the double effect refrigeration cycle can be found in the literature [32]. An MGT and ICE are other unsophisticated and straightforward method to be used as the chief mover of a residential-scale CCHP system (scenarios 3 and 2, respectively). At the combustion chamber of MGT, the fuel is mixed up with incoming air of the compressor before being expanded in the turbine. The hot gases are then used in an HRSG to create heating as in scenario 1.

Nevertheless, the ICE can create less power; it can generate more heating by the cooling water used to cool the engine to lower temperatures in scenario 2. There are some assumptions made in the modeling of the CCHP system, in which the main premises considered to model the proposed system are as follows [33, 34]:

- There is negligible heat loss from the components
- Steady-state conditions are applied
- Air and gas mixtures are modeled via ideal gas models
- Contact resistance in SOFC is neglected
- Kinetic and potential energy changes are small to consider
- Unburned gasses are fully oxidized at the exit of afterburner and combustion chambers (scenarios 2 and 3)

Modeling and analysis

In order to render the analysis of the proposed systems, thermodynamic equations (energy and exergy balance equations as well as mass balance) are solved for each component of the order (considering a control volume around the

Table 1 Summary of the literature survey highlighting the research gap

Author	Year	System	Reformer/fuel	Energy	Exergy	Exergoenvironmental analysis	Exergoeconomic	Maximum exergy efficiency	2D Multi-objective optimization	3D Multi-objective optimization
Kaldehi et al. [6]	2017	Stirling engine/CCHP	NA/NG	✓	✗	✗	✗	NA	✗	✗
Mojaver et al. [7]	2020	SOFC/CCHP	Internal/NG	✓	✓	✗	✓	48.03	✗	✗
Abbasi et al. [8]	2018	ICE-GT	NA/NG	✓	✓	✗	✓	62.8	✗	✗
Cai et al. [9]	2016	GT-CHP	NA/NG	✓	✓	✗	✗	NA	✗	✗
Mehrpouya et al. [10]	2019	SOFC-CCHP	Internal/NG	✓	✓	✓	✗	60	✗	✗
Wang et al. [11]	2017	GT-CCHP	NA/NG	✓	✗	✗	✗	NA	✗	✗
Li et al. [12]	2014	CCHP	NA/NG	✓	✗	✗	✗	NA	✗	✗
Jing et al. [13]	2017	SOFC-CCHP	Internal/NG	✓	✓	✗	✗	58	✓	✗
Abbasi et al. [14]	2018	CCHP	NA/NA	✓	✗	✗	✗	NA	✗	✗
Farahnak et al. [15]	2015	ICE -CCHP	NA/NG	✓	✗	✗	✗	NA	✗	✗
Feng et al. [16]	2019	ICE -CCHP	NA/NG	✓	✗	✗	✗	NA	✗	✗
Moghimi et al. [17]	2018	GT-CCHP	NA/NG	✓	✓	✓	✓	45.77	✓	✗
Al Moussavi et al. [18]	2017	SOFC-CCHP	Internal/NG	✓	✓	✓	✓	45.77	✗	✗
Yousefi et al. [19]	2017	ICE-CCHP	NA/NG	✓	✗	✗	✗	NA	✓	✗
Rey et al. [9]	2014	ICE-CCHP	NA/NG	✓	✗	✗	✗	NA	✗	✗
Luo et al. [20]	2017	SOFC/GT-CCHP	Internal/NG	✓	✗	✓	✗	✗	✓	✗
Chen et al. [21]	2018	PEMFC-CCHP	NA/H$_2$	✓	✓	✓	✓	39.9	✗	✗
Chitgar et al. [22]	2019	SOFC-multigenerational	Internal/NG	✓	✓	✗	✓	54	✗	✗
Present work	–	Hybrid SOFC/GT/HRSG/Li-Br	Internal/Natural gas	✓	✓	✓	✓	73.15	✓	✓

✓ Analysis is carried out

✗ Analysis is not carried out

NA Not applicable and *NG* natural gas

elements) in the package of engineering equation solver EES. Also, to find the final cost and CO_2 emission of the system, the environmental assessment, along with cost balance equations, is considered. The efficiency and the unit product cost of each scenario are regarded as the objective functions of genetic algorithms optimization code, which is developed in MATLAB.

Thermodynamic modeling

Energy and exergy balance is solved for each component to find the corresponding energy flow and exergy destruction via [35, 36]:

$$\sum \dot{m}_{in} = \sum \dot{m}_{out} \tag{1}$$

$$\dot{Q} - \dot{W} = \sum \dot{m}_{out} h_{out} - \sum \dot{m}_{in} h_{in} \tag{2}$$

$$\dot{Ex}_Q - \dot{Ex}_W = \sum \dot{m}_{out} ex_{out} - \sum \dot{m}_{in} ex_{in} + \dot{Ex}_D \tag{3}$$

in which $\dot{Ex}$ is the rate of exergy and $\dot{Q}$ and $\dot{W}$, respectively, define the rate of heat transfer and power of the control volume. There are different subsystems in the proposed CCHP system which will be discussed through the following:

SOFC system

In the SOFC system, the fuel will be reformed, so the H_2 content becomes higher in the SOFC system and so the global reaction as equation four is taken place [37]:

$$H_2 + \frac{1}{2}O_2 \rightarrow H_2O \tag{4}$$

For the reforming purposes, the internal reformer is a better choice since it will charge no additional cost to the system [33].

The two equations occurring in each cell of the stack are reforming and shifting equations, the equilibrium constant of which is [33, 38]:
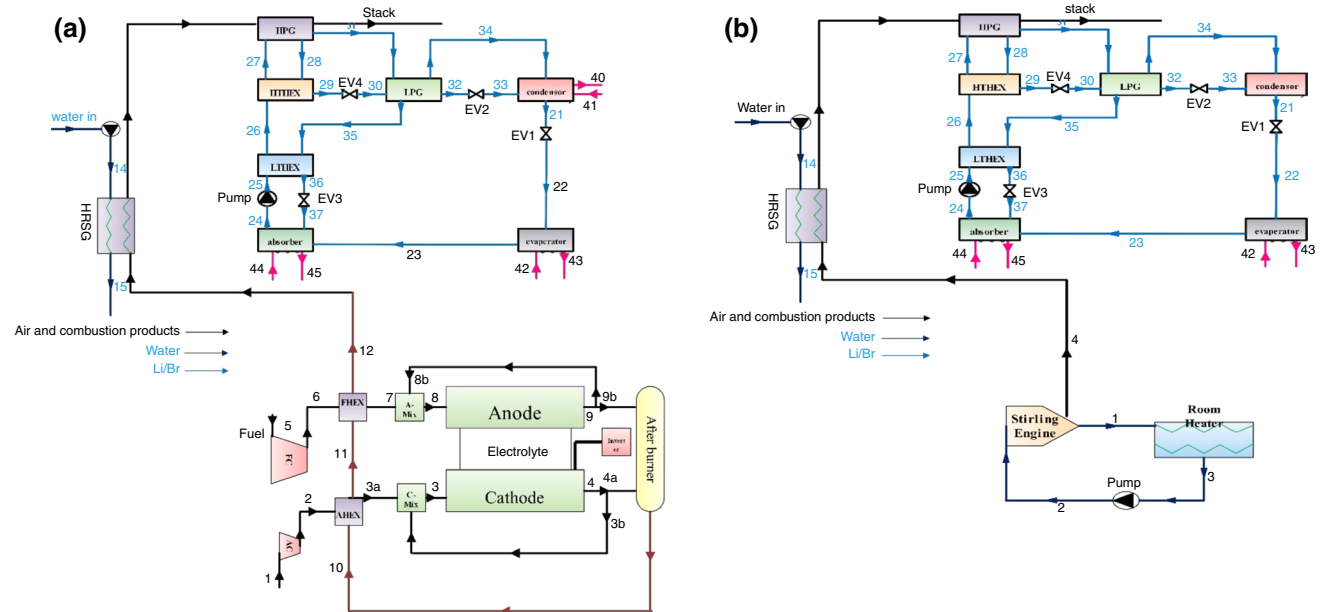
$$lnK_R = -\frac{\Delta \bar{g}_R^0}{\bar{R}T_{FC,e}} = ln\left[\frac{\left(\dot{n}_{CO} + x_r - y_r\right) \times \left(\dot{n}_{H_2} + 3x_r + y_r - z_r\right)}{\left(\dot{n}_{CH_4} + x_r\right) \times \left(\dot{n}_{H_2O} - x_r - y_r + z_r\right)} \times \frac{P^2}{n_{tot,in}^2 + 2x_r}\right] \tag{5}$$

Fig. 1 Schematic diagrams of the proposed CCHP systems for **a** scenario 1, **b** scenario 2, **c** scenario 3, **d** scenario 4
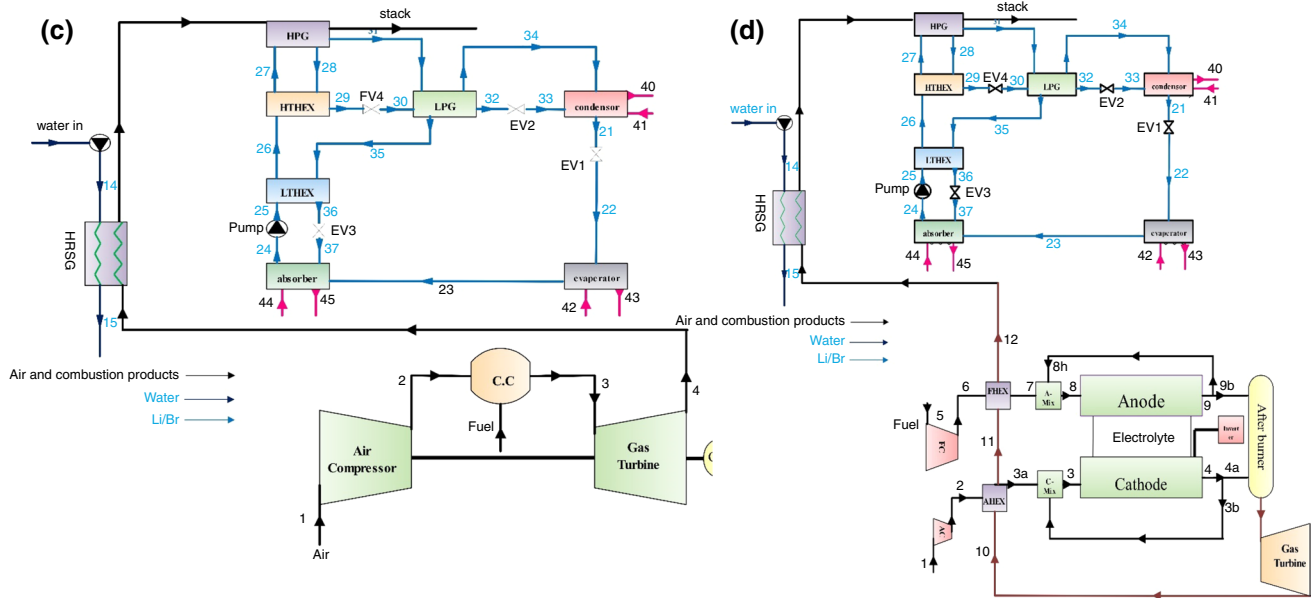
Fig. 1 (continued)

$$lnK_S = -\frac{\Delta\bar{g}_s^0}{\bar{R}T_{FC,e}} = ln\left[\frac{(\dot{n}_{CO_2} + y_r) \times (\dot{n}_{H_2} + 3x_r + y_r - z_r)}{(\dot{n}_{CO} + x_r - y_r) \times (\dot{n}_{H_2O} - x_r - y_r + z_r)}\right] \tag{6}$$

where x_r and y_r, respectively, are the reaction rate of reforming and shifting equations. Moreover, Faraday's law is used to determine the amount of hydrogen reacted according to equation four as:

$$j = \frac{n_e F z_r}{N_c A_c} \tag{7}$$

in which N_c, A_c, and n_e refer to the number of cells, area of cells, and the number of electrons transferred in the global reaction, respectively.

Furthermore, to find the reacted hydrogen, the fuel utilization factor will be written in the system of equations as [39]:

$$U_f = \frac{z_r}{\dot{n}_{H_2} + 3x_r + y_r} \tag{8}$$

Also, to find the net power output to the SOFC stack, the energy balance can be written as follows to find the gas properties at the exit of the stack:

$$\dot{W}_{SOFC,stack,DC} = mh_8 + \dot{m}h_4 - \dot{m}h_3 - \dot{m}h_7 \tag{9}$$

Also, from the electrochemical reaction, the fuel cell power is:

$$\dot{W}_{SOFC,stack,DC} = N_c A_c j V_c \tag{10}$$

$$\dot{W}_{SOFC,stack,AC} = \dot{W}_{SOFC,stack,DC} \times \eta_{inv} \tag{11}$$

in which j is the current density and V_c is the voltage of the cell and is calculated from the nominal voltage minus the losses which occur in the cell as:

$$V_c = V_N - V_{loss} \tag{12}$$

$$V_{loss} = V_{ohm} + V_{act} + V_{conc} \tag{13}$$

$$V_N = -\frac{\Delta G^0}{n_e F} - \frac{\bar{R}T_C}{n_e F}ln\left(\frac{p_{H_2O}}{p_{H_2}\sqrt{p_{O_2}}}\right) \tag{14}$$

in which V_{ohm}, V_{act}, V_{conc} is Ohmic over potential, activation overpotential, and concentration overpotential, respectively [33, 40].

Other system components

Energy and exergy balance equations for SOFC and other components like heat exchangers, compressors, pumps, and turbine, as well as expansion valves, are tabulated in Table 2 based on Eqs. 1–3.

Exergoeconomic analysis

To find a suitable option between different scenarios from an economic point of view, an exergoeconomic analysis seems necessary. Between various methods that have been

Table 2 Energy and exergy rate balances for the system components in different scenarios [41, 42]

Component	Energy balance	Exergy balance
SOFC		
SOFC	$\dot{W}_{SOFC,stack,DC} = \dot{m}h_8 + \dot{m}h_4 - \dot{m}h_3 - \dot{m}h_7$	$\dot{EX}_{D,SOFC} = \dot{EX}_7 + \dot{EX}_9 - (\dot{EX}_4 + \dot{EX}_8) - \dot{W}_{SOFC,stack,DC}$
AHX	$0 = \dot{m}h_9 + \dot{m}h_2 - \dot{m}h_{3a} - \dot{m}h_{10}$	$\dot{EX}_{D,AHX} = \dot{EX}_9 - \dot{EX}_{10} - (\dot{EX}_{3a} - \dot{EX}_2)$
Fuel blower	$\dot{W}_{F.B} = \dot{m}h_6 - \dot{m}h_5$	$\dot{EX}_{D,FC} = \dot{W}_{FC} - (\dot{EX}_6 - \dot{EX}_5)$
Air blower	$\dot{W}_{A.B} = \dot{m}h_2 - \dot{m}h_1$	$\dot{EX}_{D,AC} = \dot{W}_{AC} - (\dot{EX}_2 \text{-} \dot{EX}_1)$
Afterburner	$0 = \dot{m}h_{8b} + \dot{m}h_{4a} - \dot{m}h_9$	$\dot{EX}_{D,AB} = \dot{EX}_{4a} + \dot{EX}_{8b} - \dot{EX}_9$
Anode mixer	$0 = \dot{m}h_6 - \dot{m}h_{7b} - \dot{m}h_7$	$\dot{EX}_{D,AM} = \dot{EX}_6 + \dot{EX}_{7b} - \dot{EX}_7$
Cathode mixer	$0 = \dot{m}h_{3a} - \dot{m}h_3 - \dot{m}h_{3b}$	$\dot{EX}_{D,CM} = \dot{EX}_{3b} + \dot{EX}_{3a} - \dot{EX}_3$
ICE		
ICE	$\dot{W}_{ICE} = \eta_{pcy}(\dot{Q}_{high} - \dot{Q}_{loss})$	$\dot{EX}_{D,ICE} = \dot{EX}_{Fuel} - (\dot{EX}_2 - \dot{EX}_1 + \dot{W}_{ICE})$
MGT		
Comp.	$\dot{W}_{Comp} = \dot{m}h_2 - \dot{m}h_1$	$\dot{EX}_{D,C} = \dot{EX}_1 - \dot{EX}_2 + \dot{W}_{C1}$
C.C	$\dot{Q}_{loss} = \dot{m}h_2 - \dot{m}h_3 + mLHV_{fuel}$	$\dot{EX}_{D,CC} = \dot{EX}_2 + \dot{EX}_{fuel} - \dot{EX}_3$
GT	$\dot{W}_{GT} = \dot{m}h_4 - \dot{m}h_3$	$\dot{EX}_{D,T} = \dot{EX}_3 - \dot{EX}_4 - \dot{W}_T$
Li/Br double effect absorption chiller		
HPG	$\dot{Q}_{HPG} = \dot{m}_{11}h_{11} + \dot{m}_{32}h_{32} - \dot{m}_{31}h_{31}$	$\dot{EX}_{D,HPG} = \dot{EX}_{31} - \dot{EX}_{32} - \dot{EX}_{11} - \dot{EX}_{st.}$
LPG	$\dot{m}_{11}h_{11} + \dot{m}_{10}h_{10} - \dot{m}_{14}h_{14} - \dot{m}_{15}h_{15} - \dot{m}_{15}h_{15} = 0;$ $\dot{Q}_{LPG} = \dot{m}_{11}h_{11} - \dot{m}_{14}h_{14}$	$\dot{EX}_{D,LPG} = \dot{EX}_{11} + \dot{EX}_{10} - \dot{EX}_{12} - \dot{EX}_{14} - \dot{EX}_{15}$
Evap.	$\dot{Q}_{evap} = \dot{m}_{28}h_{28} - \dot{m}_{27}h_{27}$	$\dot{EX}_{D,evap} = \dot{EX}_{22} + \dot{EX}_{27} - \dot{EX}_{28} - \dot{EX}_{23}$
Cond.	$\dot{Q}_{cond} = \dot{m}_{14}h_{14} + \dot{m}_{13}h_{13} - \dot{m}_{26}h_{26}$	$\dot{EX}_{D,Cond} = \dot{EX}_{14} + \dot{EX}_{13} + \dot{EX}_{20} - \dot{EX}_{21} - \dot{EX}_{26}$
Abs.	$\dot{Q}_{abs} = \dot{m}_{28}h_{28} + \dot{m}_{17}h_{17} - \dot{m}_{29}h_{29}$	$\dot{EX}_{D,Abs} = \dot{EX}_{28} + \dot{EX}_{24} + \dot{EX}_{17} - \dot{EX}_{29} - \dot{EX}_{25}$
Pump	$h_{30} = h_{29} + \frac{\dot{W}_p}{\dot{m}_{29}}, \dot{W}_p = \dot{m}_{29} \times (P_{HPG} - P_{abs})/\eta_p \times \rho_{29}$	$\dot{EX}_{D,P} = \dot{EX}_{29} - \dot{EX}_{30} + \dot{W}_p$
LTHEX	$h_{16} = h_{15} - (h_{15} - h'_{16}) \times \eta_{LTHEX}$ $h_{16} = \frac{\dot{m}_{15}}{\dot{m}_{16}}(h_{15} - h_{16}) + h_{15} \; h'_{16} = h(T_{abs}, x_{15}),$	$\dot{EX}_{D,LTHEX} = \dot{EX}_{15} + \dot{EX}_{30} - \dot{EX}_{16} - \dot{EX}_{31}$
HTHEX	$h_{29} = h_{28} - (h_{28} - h'_{29}) \times \eta_{HTHEX}$ $h_{27} = \frac{\dot{m}_{28}}{\dot{m}_{26}}(h_{28} - h_{29}) + h_{26}, h'_{29} = h(T_{26}, x_{28})$	$\dot{EX}_{D,HTHEX} = \dot{EX}_{31} + \dot{EX}_{33} - \dot{EX}_{32} - \dot{EX}_{35}$
E.V	$h_i = h_e$	$\dot{EX}_{D,HTR} = \dot{EX}_i - \dot{EX}_e$

proposed (SPECO), specific costing theory is used expansively to figure out the economic aspects of energy systems.

In this method, the exergy cost of the component is determined via writing exergy balance equations and solving them simultaneously with cost balances. In order to find the exergy, the cost of each stream, auxiliary equations are applied to each component. Cost balance equations are applied to each system component as follows [43]:

$$\sum \dot{C}_{out,k} + \dot{C}_{w,k} = \sum \dot{C}_{in,k} + \dot{C}_{q,k} + \dot{Z}_k \quad (15)$$

$$\dot{Z}_k = \dot{Z}_k^{CI} + \dot{Z}_k^{OM} \quad (16)$$

$$\dot{C} = c\dot{EX} \quad (17)$$

$$\dot{C}_{out} = c_{out}\dot{EX}_{out} \quad (18)$$

$$\dot{C}_q = c_q \dot{EX}_q \quad (19)$$

$$\dot{C}_w = c_w \dot{EX}_w \quad (20)$$

in which $\dot{Z}_k^{OM}$ is the price of operation and maintenance of each component, c represents specific exergy cost, and $\dot{C}$ stands for the cost rate.

Besides, annual Levelized capital investment for the kth component is determined [44]:

$$\dot{Z}_k^{CI} = \left(\frac{CRF}{\tau}\right)Z_k \quad (21)$$

Table 3 Cost equations for components of the proposed systems [47–49]

Component	Cost equation
SOFC	
SOFC	$Z_{\text{SOFC}} = A_{\text{a}} N_{\text{FC}} (2.96 T_{\text{FC,e}} - 1907)$
AHX	$Z_{\text{AHX}} = 3 \times \left[130 \times \left(\frac{A_{\text{AHX}}}{0.093} \right)^{0.78} \right]$
Fuel and air blowers	$Z_{\text{AC}} = Z_{\text{AF}} = 91562 \times \left(\frac{\dot{W}_{\text{AC}}}{455} \right)^{0.67}$
Afterburner	$Z_{\text{AB}} = \frac{46.08 \times \dot{m}_4}{(0.955 - (P_{11}/P_4))} \left(1 + e^{0.018 T_{11} - 26.4} \right)$
Inverter	$Z_{\text{inv}} = 10^5 \times \left(\frac{\dot{W}_{\text{SOFC,DC}}}{500} \right)^{0.7}$
ICE	
ICE	$Z_{\text{ICE}} = 2200 \times \dot{W}_{\text{ICE}}$
MGT	
Comp.	$Z_{\text{AC}} = \left(\frac{75 \dot{m}_{\text{air}}}{0.9 - \eta_{\text{is,C}}} \right) \left(\frac{P_{\text{out}}}{P_{\text{in}}} \right) \ln \left(\frac{P_{\text{out}}}{P_{\text{in}}} \right)$
C.C	$Z_{\text{cc}} = 48.64 \dot{m}_{\text{air}} (1 + \exp(0.018 T_{\text{out}} - 26.4)) \frac{1}{0.995 - \frac{P_{\text{out}}}{P_{\text{in}}}}$
GT	$Z_{\text{GT}} = \left(\frac{479.34 \dot{m}_{\text{g}}}{0.92 - \eta_{\text{st}}} \right) \left(Ln \left(P_{\text{inlet}} / P_{\text{outlet}} \right) \right) \left(1 + e^{0.036 T_{\text{inlet}} - 54.4} \right)$
Li/Br double effect absorption chiller	
HPG	$Z_{\text{HPG}} = 17500 \left(\frac{A_{\text{HPG}}}{100} \right)^{0.6}$
LPG	$Z_{\text{LPG}} = 17500 \left(\frac{A_{\text{LPG}}}{100} \right)^{0.6}$
Evap.	$Z_{\text{Evap}} = 16000 \left(\frac{A_{\text{Evap}}}{100} \right)^{0.6}$
Cond.	$Z_{\text{Cond}} = 8000 \left(\frac{A_{\text{Cond}}}{100} \right)^{0.6}$
Abs.	$Z_{\text{ABS}} = 16000 \left(\frac{A_{\text{ABS}}}{100} \right)^{0.6}$
Pump	$Z_{\text{Pm}} = c_1 \dot{W}_{\text{Pm}}^{0.65}$ $c_1 = 1000 \, \$/kW^{0.65}$
LTHEX	$Z_{\text{HTHEX}} = 12000 \left(\frac{A_{\text{HTHEX}}}{100} \right)^{0.6}$
HTHEX	$Z_{\text{LTHEX}} = 12000 \left(\frac{A_{\text{LTHEX}}}{100} \right)^{0.6}$
$i_r = 0.12$, $n = 20$ years	

where τ is the total operation time of the energy system in one year, which is assumed 8000 h in this research and CRF is the capital recovery factor that can be defined as [45]:

$$\text{CRF} = \frac{i_{\text{r}} (1 + i_{\text{r}})^{\text{n}}}{(1 + i_{\text{r}})^{n} - 1} \quad (22)$$

Table 3 summarizes the cost equations(Z_{k})of the system components at the base year. Subsequently, Z_{k} for the present year (2018) is premeditated [46]:

$$\text{Cost at present year} = \text{Original cost} \times \frac{\text{CEPCI of the present year}}{\text{CEPCI of the base year}} \quad (23)$$

where i_r is the interest rate and n is the number of operating years.

In order to evaluate the system from exergoeconomic point of view, $c_{\text{F, k}}$, $c_{\text{P, k}}$, $\dot{C}_{\text{D, k}}$, $\dot{C}_{\text{L, k}}$, and f_k are illustrated as [50]:

$$c_{\text{F,k}} = \frac{\dot{C}_{\text{F,k}}}{\dot{EX}_{\text{F,k}}} \quad (24)$$

$$c_{\text{P,k}} = \frac{\dot{C}_{\text{P,k}}}{\dot{EX}_{\text{P,k}}} \quad (25)$$

Table 4 Cost balances and auxiliary equations for the components [28, 38, 51]

Component	Energy balance	Exergy balance
SOFC		
SOFC	$\dot{C}_3 + \dot{C}_9 + \dot{Z}_{SOFC,stack,PY} = \dot{C}_4 + \dot{C}_{10} + \dot{C}_{W,SOFC,stack}$	$c_4 = c_{W,SOFC,DC}$ $c_{10} = c_{W,SOFC,DC}$
AHX	$\dot{C}_2 + \dot{C}_{11} + \dot{Z}_{AHX,PY} = \dot{C}_{12} + \dot{C}_{3a}$	$c_{11} = c_{12}$
Fuel Blower	$\dot{C}_{W,FC} + \dot{C}_7 + \dot{Z}_{FC,PY} = \dot{C}_8$	$c_{W,FC} = c_{W,SOFC,AC}$
Air blower	$\dot{C}_{W,AC} + \dot{C}_1 + \dot{Z}_{AC,PY} = \dot{C}_2$	$c_1 = 0$ $c_{W,AC} = c_{W,SOFC,AC}$
Afterburner	$\dot{C}_{10b} + \dot{C}_{4a} + \dot{Z}_{AB,PY} = \dot{C}_{11}$	$c_{10b} = c_{9b}, c_{4a} = c_{3b}$ $c_{10b} = c_{10}, c_{3b} = c_4$
Anode mixer	$\dot{C}_8 + \dot{C}_{9b} + \dot{Z}_{AM,PY}(0) = \dot{C}_9$	N/A
Cathode mixer	$\dot{C}_{3b} + \dot{C}_{3a} + \dot{Z}_{CM,PY}(0) = \dot{C}_3$	N/A
Inverter	$\dot{C}_{W,SOFC,DC} + \dot{Z}_{I,PY} = \dot{C}_{W,SOFC,AC}$	N/A
ICE		
ICE	$\dot{C}_{12} + \dot{C}_{15} + \dot{Z}_{SE,PY} = \dot{C}_{14} + \dot{C}_{13} + \dot{C}_{W,SE}$	$c_{W,SE} = \left(c_{14}\dot{EX}_{14} - c_{15}\dot{EX}_{15}\right)/\left(\dot{EX}_{14} - \dot{EX}_{15}\right)$ $c_{12} = c_{13}$
MGT		
Comp.	$\dot{C}_1 + \dot{C}_{46} + \dot{Z}_{AC} = \dot{C}_2$	$c_{46} = c_{47}$
C.C	$\dot{C}_7 + \dot{C}_2 + \dot{Z}_{C.C} = \dot{C}_3$	N/A
GT	$\dot{C}_3 + \dot{Z}_{GT} = \dot{C}_3 + \dot{C}_{47}$	$c_4 = c_3$
Li/Br double effect absorption chiller		
HPG	$\dot{C}_7 + \dot{C}_{QPV} + \dot{Z}_{HPG} = \dot{C}_8 + \dot{C}_{11}$	$\dfrac{\dot{C}_{11}}{\dot{m}_{11}(ex_{11}-ex_7)} = \dfrac{\dot{C}_7(e_8-e_{11})}{\dot{m}_7(ex_{11}-ex_7)(ex_8-ex_7)} + \dfrac{\dot{C}_8}{\dot{m}_8(ex_8-ex_7)}$
LPG	$\dot{C}_{11} + \dot{C}_{10} + \dot{Z}_{LPG} = \dot{C}_{14} + \dot{C}_{15} + \dot{C}_{12}$	$\dfrac{\dot{C}_{14}}{\dot{m}_{14}(ex_{14}-xe_{10})} = \dfrac{\dot{C}_{10}(e_{15}-e_{14})}{\dot{m}_{10}(ex_{14}-ex_{10})(ex_{15}-ex_{10})} + \dfrac{\dot{C}_{15}}{\dot{m}_{15}(ex_{15}-ex_{10})}$
Cooling set	$\dot{C}_{14} + \dot{C}_{13} + \dot{Z}_{COND} = \dot{C}_1 + \Delta\dot{C}_{COND}$ $\dot{C}_3 + \dot{C}_{17} + \dot{Z}_{ABS} = \dot{C}_4 + \Delta\dot{C}_{ABS}$ $\dot{C}_{12} + \dot{C}_{14} + \dot{C}_9 + \dot{C}_{16}$ $+ \dot{Z}_{ABS} + \dot{Z}_{COND} + \dot{Z}_{EVAP} + 3\dot{Z}_{E.V} = \Delta\dot{C}_{COND} + \Delta\dot{C}_{ABS} + \dot{C}_{23} - \dot{C}_{22}$ $+ \dot{C}_4 + \dot{C}_{10}$	$\dfrac{\dot{C}_{13} + \dot{C}_{14}}{\dot{EX}_{13} + \dot{EX}_{14}} = \dfrac{\dot{C}_1}{\dot{E}_1}$ $\dfrac{\dot{C}_3 + \dot{C}_{17}}{\dot{EX}_3 + \dot{EX}_{17}} = \dfrac{\dot{C}_4}{\dot{E}_4}$ $c_1 = c_2, \ c_2 = c_3, \ c_9 = c_{10}$ $c_{12} = c_{13}, \ c_{16} = c_{17}, \ c_{22} = c_{23}$
Pump	$\dot{C}_4 + \dot{C}_{26} + \dot{Z}_{Pm} = \dot{C}_5$	$c_{19} = c_{26}$
LTHEX	$\dot{C}_6 + \dot{C}_8 + \dot{Z}_{HTHEX} = \dot{C}_7 + \dot{C}_9$	$c_8 = c_9$
HTHEX	$\dot{C}_5 + \dot{C}_{15} + \dot{C}_{34} + \dot{Z}_{LTHEX} = \dot{C}_6 + \dot{C}_{16} + \dot{C}_{35}$	$c_{15} = c_{16}$ $c_{34} = c_{35}$

$$\dot{C}_{D,k} = c_{F,k}\dot{EX}_{D,k} \tag{26}$$

$$f_k = \frac{\dot{Z}_k}{\dot{Z}_k + \dot{C}_{D,k} + \dot{C}_{L,k}} \tag{27}$$

$$r_k = \frac{c_{P,k} - c_{F,k}}{c_{F,k}} \tag{28}$$

which are defined as the unit cost of fuel, the unit cost of the product, the cost rate of exergy destruction, the cost rate of exergy loss, and the exergoeconomic factor, respectively. The exergoeconomic factor, as shown in Eq. (27),

demonstrates the importance of capital and operating and maintenance costs against exergy inefficiency costs.

Cost balances for the components and auxiliary equations are tabulated in Table 4.

Performance evaluation

In order to evaluate the performance of the system, the energy efficiency from the first law of thermodynamics, for different scenarios in the proposed CCHP system, can be defined as [43, 52]:

$$\eta_{I,a} = \frac{\dot{W}_{SOFC} - \dot{W}_{Compressors} - \dot{W}_{Pump} + \dot{Q}_{heating} + \dot{Q}_{Cooling}}{\dot{m}_F LHV_F} \tag{29}$$

$$\eta_{I,b} = \frac{\dot{W}_{ICE} - \dot{W}_{Pump} + \dot{Q}_{heating} + \dot{Q}_{Cooling}}{\dot{m}_F LHV_F} \tag{30}$$

$$\eta_{I,c} = \frac{\dot{W}_{MGT} - \dot{W}_{Pump} + \dot{Q}_{heating} + \dot{Q}_{Cooling}}{\dot{m}_F LHV_F} \tag{31}$$

$$\eta_{I,d} = \frac{\dot{W}_{SOFC} - \dot{W}_{Compressors} - \dot{W}_{Pump} + \dot{W}_{MGT} + \dot{Q}_{heating} + \dot{Q}_{Cooling}}{\dot{m}_F LHV_F} \tag{32}$$

where $\eta_{I,a\text{-}d}$ defines the first law efficiencies for the scenarios 1–4, respectively. Also $\dot{m}_F$ and LHV_F are the flow rate and lower heating value of the fuel (which is considered natural gas since its price in Iran is very low). $\dot{Q}_{heating}$ is the generated heating for domestic use by HRSG and $\dot{Q}_{cooling}$ is the amount of generated cooling via absorption chiller.

Also, to find out how the proposed system in different scenarios operates in terms of the second law of thermodynamics, the exergetic efficiency of the system for scenarios 1–4 is defined as follows, respectively [42, 53]:

$$\eta_{II,a} = \frac{\dot{W}_{net,SOFC} + \dot{EX}_{heating} + \dot{EX}_{cooling}}{\dot{EX}_F} \tag{33}$$

$$\eta_{II,b} = \frac{\dot{W}_{net,ICE} + \dot{EX}_{heating} + \dot{EX}_{cooling}}{\dot{EX}_F} \tag{34}$$

$$\eta_{II,c} = \frac{\dot{W}_{net,MGT} + \dot{E}_{heating} + \dot{E}_{cooling}}{\dot{EX}_F} \tag{35}$$

$$\eta_{II,d} = \frac{\dot{W}_{net,SOFC,MGT} + \dot{EX}_{heating} + \dot{EX}_{cooling}}{\dot{EX}_F} \tag{36}$$

in which $\dot{E}_F$ is the exergy of the fuel, which is equal to the chemical exergy of the fuel [43]. And $\dot{EX}_{heating} = \dot{EX}_{33} - \dot{EX}_{34}$ and $\dot{EX}_{cooling} = \dot{EX}_{22} - \dot{EX}_{23}$.

The total unit product cost can be achieved for the system by writing an overall cost balance to the proposed method in different scenarios as [39]:

$$c_{p,tot} = \frac{\sum_{i=1}^{n_k} \dot{Z}_k + \sum_{i=1}^{n_F} \dot{C}_{F_i}}{\sum_{i=1}^{k} \dot{EX}_{P_i}} \tag{37}$$

in which c_F is considered to be 0.04 cent m^{-3} in Iran. Furthermore, the payback period can be defined as [47]:

$$c_{p,tot} = \frac{\sum_{i=1}^{n_k} \dot{Z}_k}{\dot{W}_{net} \times \tau \times EC} \tag{38}$$

in which EC is assumed to be the electricity cost and equals to 0.1 $ kWh^{-1} in this study.

Environmental impact assessment

Using CCHP systems and efficient design of the energy systems, along with the utilization of renewable technology with low GHG emissions, results in environmental sustainability. In this manner, a sustainability index is defined in the literature, and the amount of emitted CO_2 is of prime importance in this index [54, 55]. The emitted CO_2 for different scenarios is defined via Eqs. 38–41. Also, for showing the motivation of the use of CCHP systems, the emitted CO_2 for the best case from efficiency and economic viewpoints is put to a comparison. The three considered cases for the best-case scenario are: (1) single prime mover is the sole objective of the system, and the exhaust gases are discharged to the atmosphere; (2) prime mover and HRSG for hot water production are used; (3) a CCHP system based on prime mover and HRSG along with absorption chiller is used.

$$\varepsilon_{em,1} = \frac{\dot{m}_{CO_2,emitted}}{\dot{W}_{SOFC} + \dot{Q}_{heating} + \dot{Q}_{cooling}} \tag{39}$$

$$\varepsilon_{em,2} = \frac{\dot{m}_{CO_2,emitted}}{\dot{W}_{ICE} + \dot{Q}_{heating} + \dot{Q}_{cooling}} \tag{40}$$

$$\varepsilon_{em,3} = \frac{\dot{m}_{CO_2,emitted}}{\dot{W}_{MGT} + \dot{Q}_{heating} + \dot{Q}_{cooling}} \tag{41}$$

$$\varepsilon_{em,4} = \frac{\dot{m}_{CO_2,emitted}}{\dot{W}_{SOFC,MGT} + \dot{Q}_{heating} + \dot{Q}_{cooling}} \tag{42}$$

3D optimization procedure

In designing thermal systems, many contradictory objectives need to be satisfied concurrently. When considering single-objective optimization, it is evident that to reach higher efficiency, the equipment with higher price suits well to the system performance. Also, when the price is the sole objective to be minimized, the efficiency will be sacrificed. In this study, a 3D multi-objective optimization is carried out considering to maximize exergy efficiency and minimize both the unit product cost and emissions
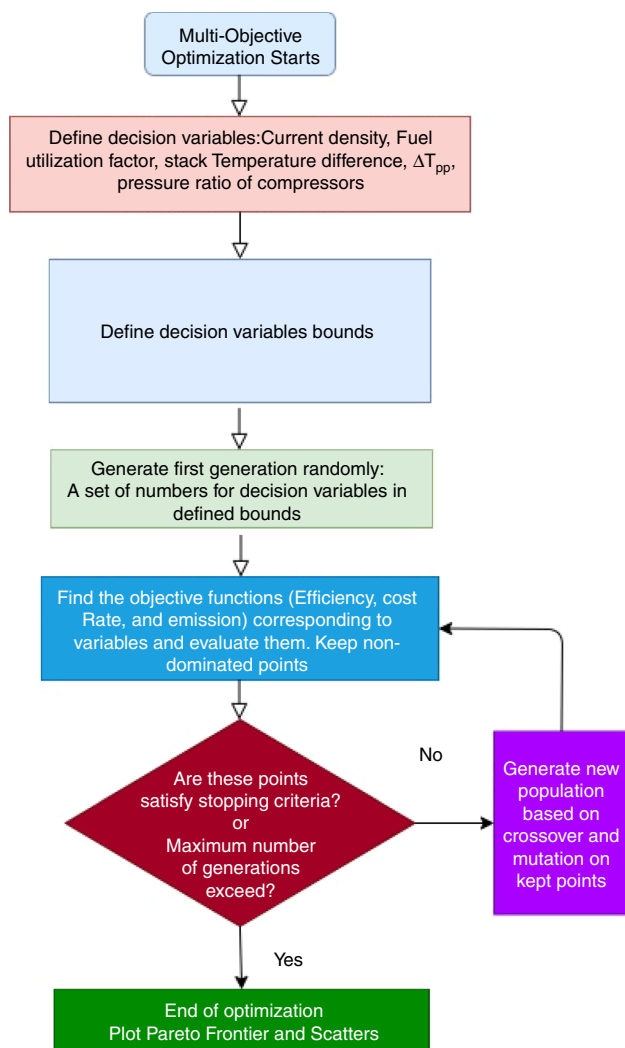
Fig. 2 Flowchart of optimization based on genetic algorithm

Table 5 Tuning parameters in the genetic algorithm optimization method

Tuning parameter	Value
Population size	350
Maximum number of generations	400
Probability of crossover	85%
Probability of mutation	1%
Selection process	Tournament
Tournament size	2

less compatible ones are crossed out. In the genetic algorithm method, the two important factors are crossover and mutation. The crossover operative mixes chromosomes as parents to produce new chromosomes called offspring. The new generations in the genetic algorithm have higher correspondence to the objective functions since in each step, genes with higher compatibility are chosen as parents. The mutation operator, however, causes chaotic variations in the structures of the genes and thus makes the optimization process away from the confined optimal.

Moreover, the tuning decision variables for multi-objective method are listed in Table 5.

Results and discussion

To find the effective critical parameters on the system performance, a parametric study is carried out in the proposed CCHP system. Also, an environmental analysis result, along with exergoeconomic results proposing exergoeconomic factors and variables, is reported. Finally, the results of Multi-objective optimization point out the best solution and the best prime mover for us.

Verification of developed models

To verify the developed thermodynamic models for each of the subsystems of the proposed CCHP system, the available data in the scientific literature are used. Validation of the SOFC and verification of the ICE are presented in Fig. 3 by comparing to the available experimental results reported by Tao et al. [58] and Hosseinpour et al. [59]. As the figure shows, the outcomes of the present study fit well on available experimental and numerical results.

Moreover, to show the accuracy of the results obtained for the double effect absorption refrigeration system in the present work, the reported data by Gomri and Hakimi are used [60]. The comparison is shown in Table 6, indicating an excellent agreement between the two sets of results.
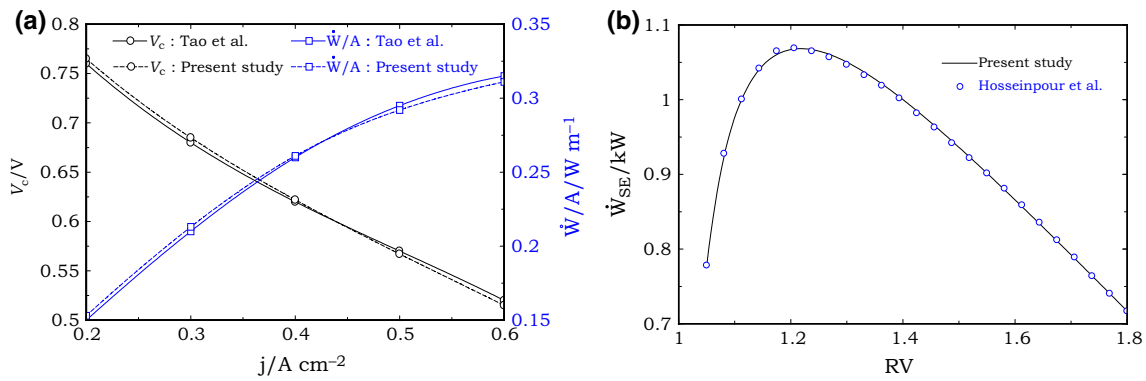
simultaneously. Neural fuzzy network code is developed in MATLAB software to get the advantage of a genetic algorithm to optimize Eqs. 33–36 (to be maximized) along with Eq. 37 and 42 (to be minimized). An optimal point is selected among a set of the optimized solution which will be given by MATLAB known as Pareto frontier [56]. The parameters and their domain in the optimization method are gathered in 3D Multi-objective optimization results section for the best-case scenario. Figure 2 indicates the flowchart of optimization carried out to reach the best solution point. Also, the genetic algorithm is an iterative method to find the ideal solution imitating the attitude of the natural evolutionary process [57]. Using a genetic algorithm, abundant populations are generated in a random manner, among which the ones having the greatest compatibility with the objective functions are selected and the

Fig. 3 **a** Validation of modeling of the SOFC modeling and **b** verification of the modeling of the ICE

Table 6 Comparison of the results obtained from the present work with experimental data for double effect absorption cycle

Constituent	Symbol	Present work/kW	Experiment/kW [60]
HP generator	$\dot{Q}_{HG}$	252.5	252.407
Condenser	$\dot{Q}_{cd}$	167.3	167.205
Evaporator	$\dot{Q}_{Ev}$	300	300
Absorber	$\dot{Q}_{ab}$	385.3	385.236
Pump	$\dot{W}$	0.054	0
	COP	1.188	1.189
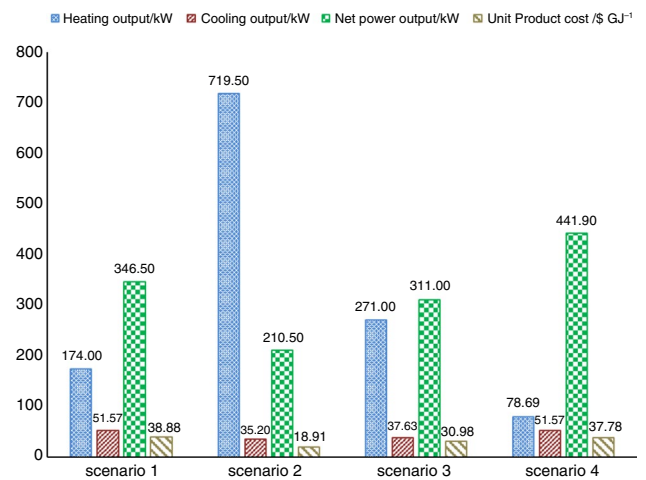
Fig. 5 Comparison of the unit product cost, generated power, heating, and cooling in different scenarios
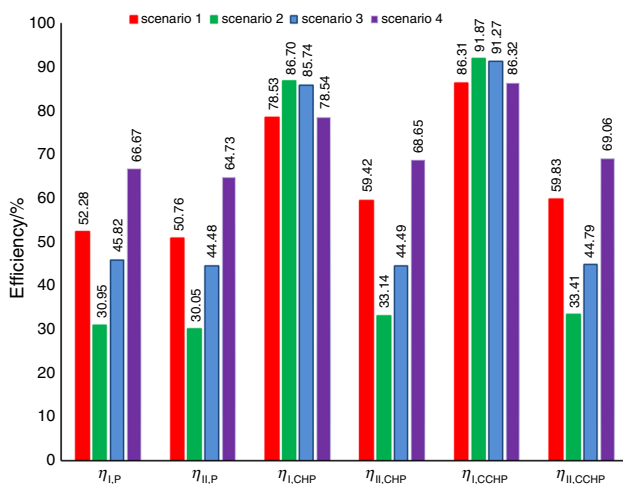
Fig. 4 Comparison of efficiencies for power production, CHP system and CCHP system in four different scenarios

Comparative study results

In order to evaluate the best proposed CCHP system, the efficiencies of each scenario for the power production system, the CHP system, and the CCHP system are, respectively,

demonstrated in Fig. 4. Also, the generated power, heating, and cooling, as well as unit product cost of different scenarios, are presented in Fig. 5. Taking Fig. 4 into consideration, it is evident that considering only the power production system, scenario 4 has the most energetic and exergetic efficiency, namely 66.67% and 64.73%, respectively. Scenario 4 is capable of producing 441.9 kW net power output, and the scenarios 1, 3, and 2 are in the next positions with 346.5 kW, 311 kW, and 210.5 kW, respectively. According to Fig. 5, the power production in different cases is all the more reason that scenario 4 indicates more energetic and exergetic efficiency. Another essential aspect of Fig. 5 is the energetic and exergetic efficiencies of different cases when the CHP system is considered. Since the energetic efficiency considers the quantity of energies and not the qualities, the energetic efficiency of scenario 2 is the highest efficiency among the cases with 86.7%, which is because it can generate 719.5 kW heating capacity. Moreover, the MGT system produces 271 kW heating, which is more than 174 kW in
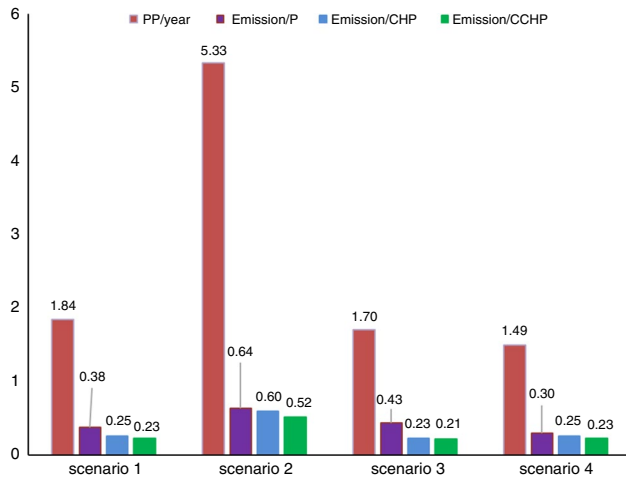
Fig. 6 Comparison of payback period and emission reduction in different scenarios

scenario 1 and 78.69 kW in scenario 4. Besides, the exergetic efficiency in scenario 4 is 68.65%, which is more than in other cases, since the power generation, in this case, is higher. The last but not the least important aspect of Fig. 5 is energetic and exergetic efficiency of the CCHP system in 4 cases. Considering the energetic efficiency, scenario 2 is the most efficient system with an efficiency of 91.87%. The hybrid SOFC/GT system operates better in terms of exegetic efficiency, with an efficiency of 69.06%.

The conclusion from Figs. 3 and 4 is that hybrid SOFC/GT system operates better in terms of power generation, and considering the second law efficiency, it has the highest efficiency. It is noteworthy that scenario 2 generates more heating than other cases, and it is the best case when more steam is required. Another important aspect of Fig. 4

is the unit product cost in different cases. According to Eq. (37), the more exergy of products is, the cheaper the unit product of the system becomes. Also, more equipment in the system causes the nominator of Eq. (37) to become larger. The unit product cost in scenarios 1–4 is 38.88 ($ GJ^{-1}), 18.91($ GJ^{-1}), 30.98($ GJ^{-1}), and 37.78($ GJ^{-1}), respectively.

Figure 6 indicates the comparison of emission in power generation system, CHP, and CCHP system along with the payback period in four different scenarios. According to Eqs. (39–42), emission in the CCHP system becomes less than the power generation system and CHP system, which is an excellent motivation to use the CCHP system. Scenario 4 indicates the fastest payback period among the other cases with 1.49 years, while scenario 2 has the longest payback period of 5.33. Additionally, the power generation, CHP and CCHP emissions for hybrid SOFC/GT are 0.30 (ton/MWh), 0.25 (ton/MWh), and 0.23 (ton/MWh), respectively.

To investigate the systems from exergy and exergoeconomic points of view, the exergy indicator parameters like exergy destruction, the exergy of fuel, exergy of product, and lost exergy are presented as exergy indicators. Besides, the cost of components, cost of fuel, and cost of product along with destructed cost and lost cost are illustrated as exergoeconomic indicators in Tables 7 8, 9, 10 for different cases, respectively. According to tables, in scenario 1, AHE, SOFC, and AB with exergy destruction of 120 kW, 52.16 kW, and 42.62 kW, respectively, have the highest exergy destruction rate. These values are the same for scenario 4. This is due to the fact that in SOFC and A.B, there is all three primary source of irreversibility in the system, which is chemical reaction, mixing, and temperature difference. Moreover, because of the very high temperature difference in AHE, the exergy destruction in this component is higher than the

Table 7 Exergy and exergoeconomic parameters of scenario 1

	$\dot{EX}_D$/kW	$\dot{EX}_F$/kW	$\dot{EX}_P$/kW	$\dot{EX}_L$/kW	Cost/$ h^{-1}	C_f/$ GJ^{-1}	C_p/$ GJ^{-1}	C_D/$ h^{-1}	C_L/$ h^{-1}	f/%
AHE	120.00	385.60	245.80	0.00	4.50	9.35	15.19	4.04	0.00	10.26
SOFC	52.16	1333.0	1269.60	0.00	10.57	6.08	8.37	1.14	0.00	89.20
AB	42.62	544.00	501.30	0.00	1.77	8.37	9.35	1.29	0.00	27.27
HRSG	20.07	79.08	59.01	0.00	2.15	9.35	13.67	0.68	0.00	11.20
FHE	8.07	19.74	11.67	0.00	0.28	9.35	16.02	0.27	0.00	2.92
CS	7.11	8.51	2.83	0.00	0.26	8.51	26.00	0.22	0.00	19.96
AC	3.01	15.90	12.89	0.00	0.44	8.63	18.19	0.09	0.00	78.89
HPG	2.80	14.66	11.81	21.99	1.24	0.00	0.18	0.00	1.23	100.0
HTHEX	1.49	6.83	5.34	0.00	0.05	1.93	4.48	0.01	0.00	78.85
LPG	1.27	4.98	3.72	0.00	0.01	0.46	1.00	0.00	0.00	70.31
LTHEX	0.59	1.97	1.37	0.00	0.03	0.88	6.71	0.00	0.00	93.47
FC	0.06	0.43	0.37	0.00	0.03	8.63	60.28	0.00	0.00	94.20
Pump HRSG	0.04	0.17	0.12	0.00	0.01	8.63	38.30	0.00	0.00	90.29
Pump	0.00	5.00	5.00	0.00	0.01	0.16	10.12	0.00	0.00	100.0

Table 8 Exergy and exergoeconomic parameters of scenario 2

	$\dot{EX}_D$/kW	$\dot{EX}_F$/kW	$\dot{EX}_P$/kW	$\dot{EX}_L$/kW	Cost/\$ h^{-1}	C_f/\$ G^{-1}	C_P/\$ GJ^{-1}	C_D/\$ h^{-1}	C_L/\$ h^{-1}	f/%
ICE	132.40	358.40	226.00	0.00	98.76	155.20	260.20	73.99	0.00	11.54
CS	3.88	5.81	1.93	0.00	4.04	4.68	4.72	4.00	0.00	1.34
HPG	1.90	9.99	8.09	4.11	0.01	0.00	0.01	0.00	2.3	100.0
HRSG	1.14	5.74	4.59	0.00	27.26	155.20	180.40	0.64	0.00	97.65
HTHEX	1.02	4.66	3.64	0.00	0.18	0.64	0.68	0.14	0.00	21.66
LPG	0.86	3.39	2.54	0.00	0.02	0.08	0.08	0.02	0.00	20.12
LTHEX	0.40	1.34	0.94	0.00	0.04	0.04	0.06	0.01	0.00	71.43
HRSG pump	0.12	0.13	0.01	0.00	0.00	0.26	0.40	0.00	0.00	39.28
Pump	0.00	5.00	5.00	0.00	0.00	4.68	4.71	0.00	0.00	100.0

Table 9 Exergy and exergoeconomic parameters of scenario 3

	$\dot{EX}_D$/kW	$\dot{EX}_F$/kW	$\dot{EX}_P$/kW	$\dot{EX}_L$/kW	Cost/\$ h^{-1}	C_f/\$ GJ^{-1}	C_P/\$ GJ^{-1}	C_D/\$ h^{-1}	C_L/\$ h^{-1}	f/%
CC	198.80	743.90	545.00	0.00	21.2	1.098	155.2	1.256	0.00	10.26
HRSG	143.60	143.72	92.07	0.00	11.92	5.97	9.56	5.92	0.00	74.35
GT	34.94	393.20	358.30	0.00	8.65	130.6	143	5.34	0.00	69.3
CS	5.19	6.21	2.07	0.00	7.69	4.21	4.05	3.44	0.00	15.67
AC	2.76	46.50	43.73	0.00	3.21	9.94	12.65	4.98	0.00	78.89
HPG	1.46	10.68	8.65	26.10	0.01	0	0.068	0	2.04	100.0
HTHEX	1.09	4.98	3.90	0.00	0.04	0.13	0.15	0.026	0.00	43.09
LPG	0.92	3.63	2.71	0.00	0.01	0.070	0.071	0.017	0.00	52.31
LTHEX	0.43	1.43	1.00	0.00	0.068	0.032	0.053	0.0092	0.00	80.45
HRSG pump	0.06	0.26	0.19	0.00	0.25	0.23	0.36	0.0027	0.00	38.28
Pump	0.00	4.00	5.00	0.00	0.02	1.0158	1.089	0	0.00	100.0

Table 10 Exergy and exergoeconomic parameters of scenario 4

	$\dot{EX}_D$/kW	$\dot{EX}_F$/kW	$\dot{EX}_P$/kW	$\dot{EX}_L$/kW	Cost/\$ h^{-1}	C_f/\$ GJ^{-1}	C_P/\$ G J^{-1}	C_D/\$ h^{-1}	C_L/\$ h^{-1}	f/%
AHE	120.00	385.60	245.80	0.00	4.50	9.35	15.19	4.04	0.00	10.26
SOFC	52.16	1333.0	1269.60	0.00	10.57	6.08	8.37	1.14	0.00	89.20
AB	42.62	544.00	501.30	0.00	1.77	8.37	9.35	1.29	0.00	27.27
HRSG	20.07	79.08	59.01	0.00	2.15	9.35	13.67	0.68	0.00	81.20
FHE	8.07	19.74	11.67	0.00	0.28	9.35	16.02	0.27	0.00	2.92
CS	7.11	8.51	2.83	0.00	0.26	8.51	26.00	0.22	0.00	19.96
GT	5.97	101.30	95.30	0.00	0.73	9.35	11.46	3.41	0.00	72.30
IAC	3.01	15.90	12.89	0.00	0.44	8.63	18.19	0.09	0.00	78.89
HPG	2.80	14.66	11.81	15.43	1.24	0.00	0.18	0.00	1.18	100.0
HTHEX	1.49	6.83	5.34	0.00	0.05	1.93	4.48	0.01	0.00	78.85
LPG	1.27	4.98	3.72	0.00	0.01	0.46	1.00	0.00	0.00	70.31
LTHEX	0.59	1.97	1.37	0.00	0.03	0.88	6.71	0.00	0.00	93.47
FC	0.06	0.43	0.37	0.00	0.03	8.63	60.28	0.00	0.00	94.20
Pump HRSG	0.04	0.17	0.12	0.00	0.01	8.63	38.30	0.00	0.00	90.29
Pump	0.00	5.00	5.00	0.00	0.01	0.16	10.12	0.00	0.00	100.0

others. In the case of ICE and MGT, the engine and combustion chamber have the highest exergy destruction rate, which is 132.4 kW and 198.8 kW, respectively. Additionally,

it is noteworthy that the last column of Tables 5–8 is the exergoeconomic factor (f). A low value of this factor calculated for a significant component suggests that cost-saving
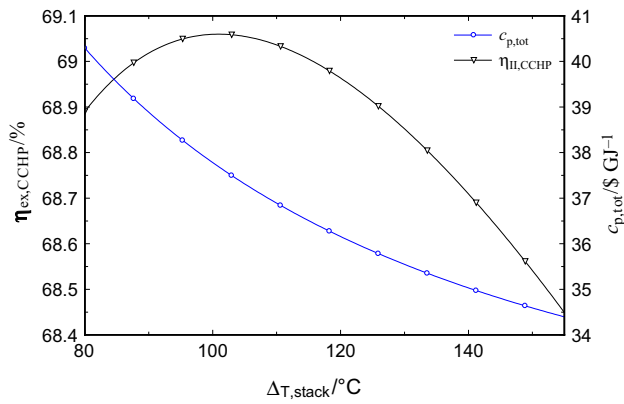
Fig. 7 Effect of stack temperature difference on exergy efficiency and unit product cost of the system in scenario 4
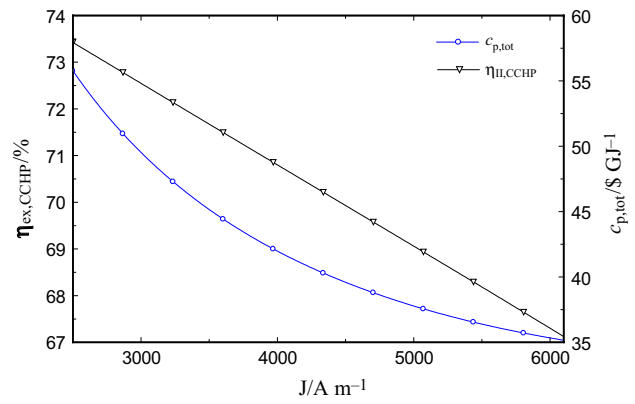

Fig. 9 Effect of current density on exergy efficiency and unit product cost of the system in scenario 4
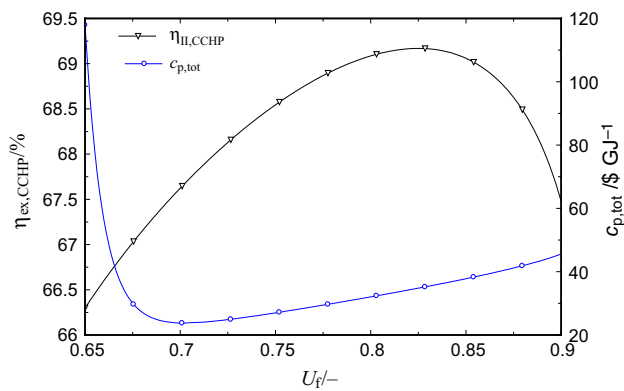

Fig. 8 Effect of fuel utilization factor on exergy efficiency and unit product cost of the system in scenario 4
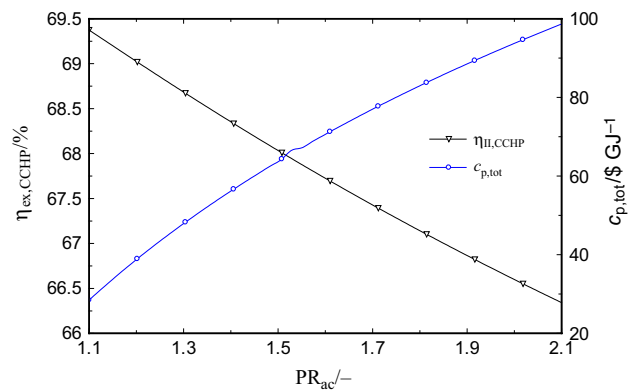

Fig. 10 Effect of air compressor pressure ratio on exergy efficiency and unit product cost of the system in scenario 4

in the entire system might be achieved by improving the component efficiency (reducing exergy destruction) even if the capital investment for the component will increase. So, it is evident that in the system, FHE and AHE have very low exergoeconomic factors, which are 2.92% and 10.26% for scenarios 1 and 4. These values are 1.34% for cooling set in scenario 2 and 10.26 for the combustion chamber in scenario 3. On the other hand, a high value of this factor suggests a decrease in the investment cost of this component at the expense of its exergetic efficiency (like fuel compressor in cases 1 and 4).

Parametric study results

The effect of crucial decision variables on the system performance indexes which are exergetic efficiency and unit product cost is indicated in this section, for the scenario number 4, which is proved to be the better case study among the other proposed cases.

Figure 7 depicts the effect of stack temperature difference on exergy efficiency and unit product cost. Increasing stack temperature difference has a positive effect on unit product cost and reduces the cost from 40.43 (S/GJ) to 34.38 (S/GJ). However, the change in exergetic efficiency is not much, and after reaching a maximum of 69.07% at 102 °C, it reduces to 68.46%. This is mainly due to the fact that increasing stack temperature difference results in a reduction in power output and an increase in heating capacity since the outlet enthalpy of the SOFC is higher.

Fuel utilization factor is another crucial design parameter, the effect of which on exergetic efficiency and unit product cost is shown in Fig. 8. Increasing fuel utilization factor from 0.65 to 0.9 causes a maximum in exergy efficiency in $U_f = 0.83$, corresponding to a value of 69.2%. Also, a minimum of 23.6 (\$ GJ^{-1}) is reached for unit product cost at the fuel utilization factor of 0.68, which makes this parameter more critical form the multi-objective optimization viewpoint.
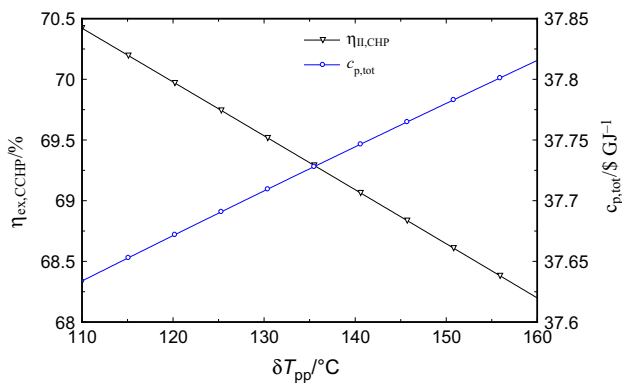
Fig. 11 Effect of pinch point temperature difference in exergy efficiency and unit product cost of the system in scenario 4

Table 11 Domain of major decision parameters

Parameter	Range
ΔT_{stack}/°C	$80 < \Delta T_{stack} < 150$
PR_{ac}	$1.1 < PR_{ac} < 2.1$
J/A m^{-2}	$2500 < J < 6100$
U_f	$0.65 < U_f < 0.9$
ΔT_{pp}/°C	$150 < \Delta T_{pp} < 200$

Fig. 12 Distribution of the 3D Pareto optimal solutions for exergy efficiency, CO_2 emission, and unit product cost of the system

The effect of the current density of SOFC on exergy efficiency and unit product cost is indicated in Fig. 9. Increasing current density from 2500 (A m^{-2}) to 6100 (A m^{-2}) results in a decrease in exergy efficiency from 73.4 to 67.1%. This is mainly because cell voltage decreases, and therefore, power output from the SOFC decreases as a result of an increase in the current density. Also, this increase causes a reduction in unit product cost from 55.08 ($ GJ^{-1}) to 35.01 ($ GJ^{-1}).

One of the crucial decision variables on system performance is the pressure ratio of air compressor, which is also equal to the value of the fuel compressor, pressure ratio, the effect of which is indicated in Fig. 10. According to this figure, when the value of PR_{ac} is raised from 1.1 to 2.1, the exergy efficiency decreases, and unit product cost increases from 69.4 to 66.3% and 27.1($ GJ^{-1}) to 98.02 ($ GJ^{-1}), respectively. This trend is primarily because increasing the pressure ratio of the compressors requires more power input to the compressors.

The last but not the least important parameter to study is the effect of pinch point temperature difference in the variation in unit product cost and exergy efficiency, which is presented in Fig. 11. As was anticipated, rising pinch point temperature difference has a negative effect on heating capacity and, thus, on overall exergy efficiency and unit product cost. Furthermore, increasing pinch point temperature difference about 50 °C causes a reduction in exergy efficiency, about 2.1%, and an increase in unit product cost about 0.5%.

3D Multi-objective optimization results

By considering the overall exergy efficiency, CO_2 emission, and the total unit product cost as the objective parameters, a multi-objective optimization is applied by using MATLAB software. Five decision parameters, along with their ranges, are listed in Table 11.

The optimal solution points of the system are illustrated in Fig. 12 as a Pareto frontier solution. As a result of multi-objective optimization to maximize exergy efficiency and minimize unit product cost and CO_2 emission, a 3-dimensional Pareto Frontier is presented in Fig. 12, which is a fitted surface to the optimum results of optimization. The ideal point of the Pareto Frontier is specified in the figure, and it has an exergy efficiency of 73.15%, unit product cost
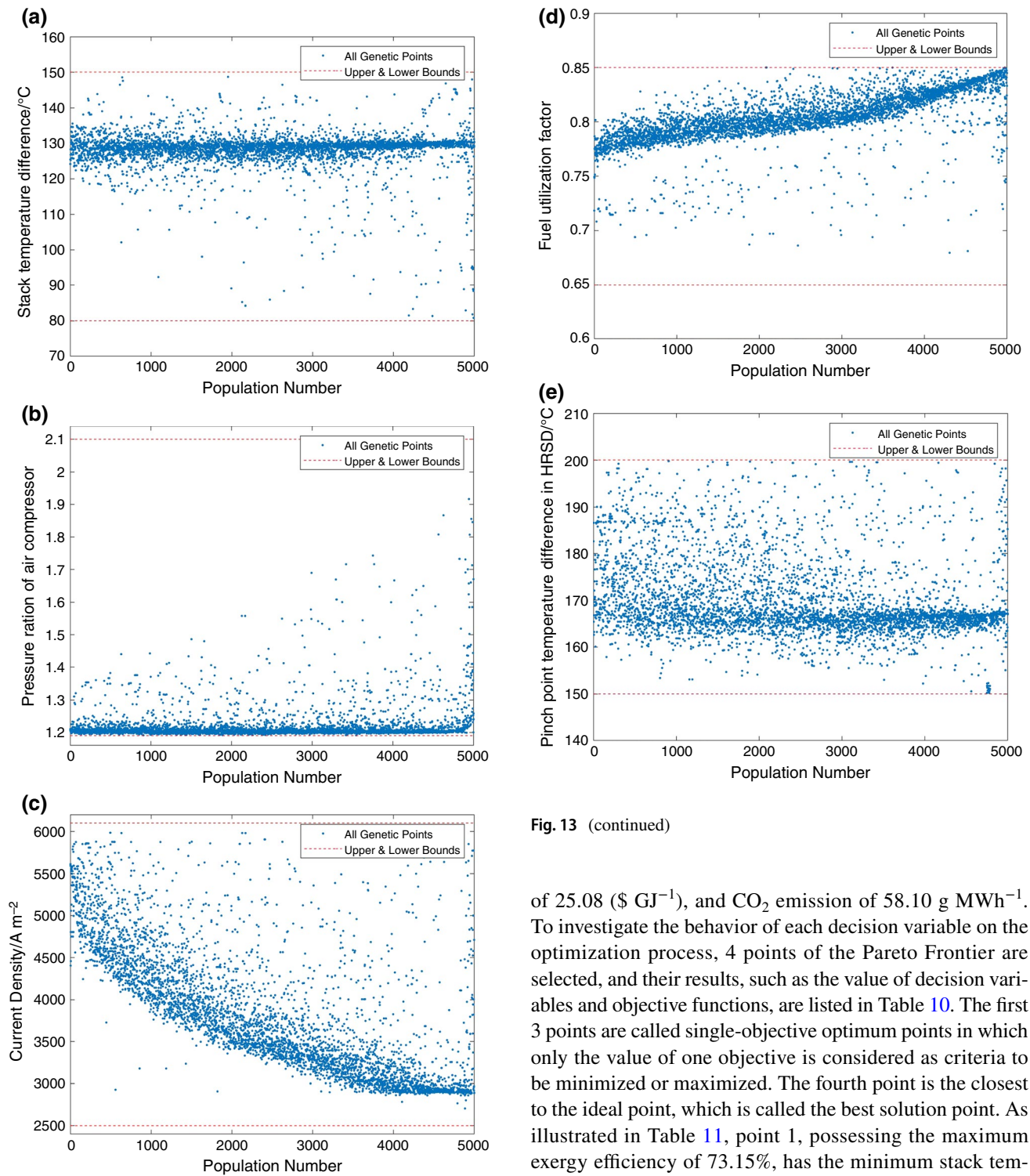
Table 12 Pareto frontier selected points with decision variables and objective functions value

	Point description	ΔT_{stack}/°C	PR_{fc}	J/A m^{-2}	U_f	ΔT_{pp}/°C	$\eta_{II, tot}$/%	$C_{P,tot}$/$ GJ^{-1}	CO_2 emission/g MWh^{-1}
1	Max efficiency	85.09	1.20	2570.23	0.87	155.47	73.15	61.01	63.10
2	Min cost	88.37	1.23	5450.15	0.69	176.30	66.44	25.08	60.80
3	Min emission	138.38	2.05	4662.01	0.69	152.16	66.11	124.43	58.10
4	Best point	91.77	1.24	2763.29	0.86	158.68	72.57	62.12	62.52

Fig. 13 Scatter distribution of decision variables with Pareto frontier: **a** stack temperature difference, **b** pressure ratio of air compressor, **c** current density, **d** fuel utilization factor, **e** pinch point temperature difference

Fig. 13 (continued)

of 25.08 (\$ GJ^{-1}), and CO_2 emission of 58.10 g MWh^{-1}. To investigate the behavior of each decision variable on the optimization process, 4 points of the Pareto Frontier are selected, and their results, such as the value of decision variables and objective functions, are listed in Table 10. The first 3 points are called single-objective optimum points in which only the value of one objective is considered as criteria to be minimized or maximized. The fourth point is the closest to the ideal point, which is called the best solution point. As illustrated in Table 11, point 1, possessing the maximum exergy efficiency of 73.15%, has the minimum stack temperature difference (85.09 K), pressure ratio of (1.20), current density of 2570.23 A m^{-2}, and fuel utilization factor of 0.87, which shows that the lower amount of these parameters leads the system to a higher amount of exergy efficiency.

However, the fuel utilization factor (U_f) has a reverse effect on the efficiency, and the higher amount of $U_f = 0.87$ results in maximum efficiency. If the unit product cost is selected as the only objective to be minimized, point 2 is the optimum point of the total cost rate of 25.08 (\$ GJ^{-1}). According to Table 12, the higher values of pinch point temperature difference cause lower values of the unit product cost. Point 3 is the point with the lowest CO_2 emission of 58.10 (g/MWh). Stack temperature difference has a reverse effect on the emission in the way that increasing the Stack temperature difference reduces the emission.

To have a better overview of the decision variables, the scattered distribution of these parameters is depicted in Fig. 13. From data in Fig. 13a, it can be seen that all the optimal points of stack temperature difference are located nearly between 120 and 140. This means that if stack temperature difference is around 130 °C, the optimum solution can be reached. Figure 13b shows the distribution of the pressure ratio of air compressors and reveals that keeping this parameter at its lowest value results in better optimization outcomes. These results also are shown in Fig. 8 in the parametric study section, which shows that increasing the pressure ratio of air compressor leads to the exergy efficiency decreasing and unit product cost increasing. Figure 13c, d and e reveals that current density, fuel utilization factor, and pinch point temperature difference have scattered distributions in their allowable domain. Current density tends to have lower values around 3000 A m^{-2}, and fuel utilization factor shall be above 0.75 to get an optimal solution. Moreover the selected optimal range for pinch point temperature difference is around 165 °C.

Conclusions

In this research paper, four different scenarios are proposed for producing, heating, cooling, and power in a small residential scale. The proposed systems are studied from viewpoints of energy, exergy, exergoeconomic, and environmental impact. The superior prime mover for the integrated system is selected to be optimized, considering exergetic efficiency and unit product cost as two main objectives. Three-objective optimization is carried out to find the maximum of exergy efficiency and a minimum of unit product cost and CO_2 emission. Main findings of the present study, as well as multi-objective optimization results, are as follows:

- Results demonstrate that the hybrid SOFC/GT system proves to be better in terms of exergetic efficiency and payback period, which is 69.06% and 1.49 years, respectively.

- ICE proves to be the better system in terms of heating generation and unit product cost, which is 719.50 kW and 18.91 (\$ GJ^{-1}).
- The parametric study shows that for specific values of fuel utilization factor, the efficiency increases and unit product cost decreases, which is of great importance for optimization purposes.
- Results show that using CCHO system demonstrates a great motivation in reducing the GHG emission.
- Optimization results show that maximum exergy efficiency for the best case can be reached higher costs, respectively, at 73.15% and 61.1 (\$ GJ^{-1}).
- Moreover, the minimum cost can be reached to the hybrid SOFC/GT system at 29.02 (\$ GJ^{-1}), which corresponds to the efficiency of 66.44%.
- The best solution points based on five decision parameters are 73.15% in exergetic efficiency, 25.08 \$ GJ^{-1} in unit product cost, and 58.10 (g MWh^{-1}) of CO_2 emission.

Compliance with ethical standards

References

1. Rahmati A, Varedi-Koulaei SM, Ahmadi MH, Ahmadi H. Dimensional synthesis of the Stirling engine based on optimizing the output work by evolutionary algorithms. Energy Rep. 2020;6:1468–86. https://doi.org/10.1016/J.EGYR.2020.05.030.
2. Motahar S, Bagheri-Esfeh H. Artificial neural network based assessment of grid-connected photovoltaic thermal systems in heating dominated regions of Iran. Sustain. Energy Technol. Assess. 2020;39:100694. https://doi.org/10.1016/J.SETA.2020.100694.

3. Safari F, Javani N, Yumurtaci Z. Hydrogen production via supercritical water gasification of almond shell over algal and agricultural hydrochars as catalysts. Int J Hydrogen Energy. 2018;43:1071–80. https://doi.org/10.1016/J.IJHYDENE.2017.05.102.

4. Gholamian E, Mahmoudi SMS, Zare V. Proposal, exergy analysis and optimization of a new biomass-based cogeneration system. Appl Therm Eng. 2016;93:223–35. https://doi.org/10.1016/j.applthermaleng.2015.09.095.

5. Kaldehi BJ, Keshavarz A, Pirooz AAS, Batooei A, Ebrahimi M. Designing a micro Stirling engine for cleaner production of combined cooling heating and power in residential sector of different climates. J Clean Prod. 2017;154:502–16. https://doi.org/10.1016/j.jclepro.2017.04.006.

6. Mojaver P, Khalilarya S, Chitsaz A, Assadi M. Multi-objective optimization of a power generation system based SOFC using Taguchi/AHP/TOPSIS triple method. Sustain Energy Technol Assess. 2020;38:100674. https://doi.org/10.1016/J.SETA.2020.100674.

7. Abbasi M, Chahartaghi M, Hashemian SM. Energy, exergy, and economic evaluations of a CCHP system by using the internal combustion engines and gas turbine as prime movers. Energy Convers Manag. 2018;173:359–74. https://doi.org/10.1016/J.ENCONMAN.2018.07.095.

8. Cai B, Li H, Hu Y, Zhang G. Operation strategy and suitability analysis of CHP system with heat recovery. Energy Build. 2017;141:284–94. https://doi.org/10.1016/j.enbuild.2017.02.056.

9. Mehrpooya M, Sadeghzadeh M, Rahimi A, Pouriman M. Technical performance analysis of a combined cooling heating and power (CCHP) system based on solid oxide fuel cell (SOFC) technology—a building application. Energy Convers Manag. 2019;198:111767. https://doi.org/10.1016/J.ENCONMAN.2019.06.078.

10. Wang Z, Han W, Zhang N, Liu M, Jin H. Proposal and assessment of a new CCHP system integrating gas turbine and heat-driven cooling/power cogeneration. Energy Convers Manag. 2017;144:1–9. https://doi.org/10.1016/J.ENCONMAN.2017.04.043.

11. Li L, Mu H, Gao W, Li M. Optimization and analysis of CCHP system based on energy loads coupling of residential and office buildings. Appl Energy. 2014;136:206–16. https://doi.org/10.1016/J.APENERGY.2014.09.020.

12. Jing R, Wang M, Brandon N, Zhao Y. Multi-criteria evaluation of solid oxide fuel cell based combined cooling heating and power (SOFC-CCHP) applications for public buildings in China. Energy. 2017;141:273–89. https://doi.org/10.1016/J.ENERGY.2017.08.111.

13. Abbasi MH, Sayyaadi H, Tahmasbzadebaie M. A methodology to obtain the foremost type and optimal size of the prime mover of a CCHP system for a large-scale residential application. Appl Therm Eng. 2018;135:389–405. https://doi.org/10.1016/j.applthermaleng.2018.02.062.

14. Petreanu I, Ebrasu D, Sisu C, Varlam M. Thermal analysis of sulfonated polymers tested as polymer electrolyte membrane for PEM fuel cells. J Therm Anal Calorim. 2012;110:335–9. https://doi.org/10.1007/s10973-012-2442-z.

15. Singh OK. Combustion simulation and emission control in natural gas fuelled combustor of gas turbine. J Therm Anal Calorim. 2016;125:949–57. https://doi.org/10.1007/s10973-016-5472-0.

16. Farahnak M, Farzaneh-Gord M, Deymi-Dashtebayaz M, Dashti F. Optimal sizing of power generation unit capacity in ICE-driven CCHP systems for various residential building sizes. Appl Energy. 2015;158:203–19. https://doi.org/10.1016/J.APENERGY.2015.08.050.

17. Feng L, Dai X, Mo J, Shi L. Performance assessment of CCHP systems with different cooling supply modes and operation strategies. Energy Convers Manag. 2019;192:188–201. https://doi.org/10.1016/J.ENCONMAN.2019.04.048.

18. Moghimi M, Emadi M, Ahmadi P, Moghadasi H. 4E analysis and multi-objective optimization of a CCHP cycle based on gas turbine and ejector refrigeration. Appl Therm Eng. 2018;141:516–30. https://doi.org/10.1016/J.APPLTHERMALENG.2018.05.075.

19. Lara Y, Petrakopoulou F, Morosuk T, Boyano A, Tsatsaronis G. An exergy-based study on the relationship between costs and environmental impacts in power plants. Energy. 2017;138:920–8. https://doi.org/10.1016/J.ENERGY.2017.07.087.

20. Ansarinasab H, Mehrpooya M, Sadeghzadeh M. An exergy-based investigation on hydrogen liquefaction plant-exergy, exergoeconomic, and exergoenvironmental analyses. J Clean Prod. 2019;210:530–41. https://doi.org/10.1016/J.JCLEPRO.2018.11.090.

21. Ahmadi MH, Nazari MA, Sadeghzadeh M, Pourfayaz F, Ghazvini M, Ming T, Meyer JP, Sharifpur M. Thermodynamic and economic analysis of performance evaluation of all the thermal power plants: a review. Energy Sci Eng. 2019;7:30–65. https://doi.org/10.1002/ese3.223.

22. Al Moussawi H, Fardoun F, Louahlia H. 4-E based optimal management of a SOFC-CCHP system model for residential applications. Energy Convers Manag. 2017;151(2017):607–29. https://doi.org/10.1016/j.enconman.2017.09.020.

23. Yousefi H, Ghodusinejad MH, Kasaeian A. Multi-objective optimal component sizing of a hybrid ICE+PV/T driven CCHP microgrid. Appl Therm Eng. 2017;122:126–38. https://doi.org/10.1016/J.APPLTHERMALENG.2017.05.017.

24. Rey G, Ulloa C, Cacabelos A, Barragáns B. Performance analysis, model development and validation with experimental data of an ICE-based micro-CCHP system. Appl Therm Eng. 2015;76:233–44. https://doi.org/10.1016/J.APPLTHERMALENG.2014.10.087.

25. Luo XJ, Fong KF. Development of multi-supply-multi-demand control strategy for combined cooling, heating and power system primed with solid oxide fuel cell-gas turbine. Energy Convers Manag. 2017;154:538–61. https://doi.org/10.1016/J.ENCONMAN.2017.11.032.

26. Chen X, Zhou H, Li W, Yu Z, Gong G, Yan Y, Luo L, Wan Z, Ding Y. Multi-criteria assessment and optimization study on 5 kW PEMFC based residential CCHP system. Energy Convers Manag. 2018;160:384–95. https://doi.org/10.1016/J.ENCONMAN.2018.01.050.

27. Chitgar N, Emadi MA, Chitsaz A, Rosen MA. Investigation of a novel multigeneration system driven by a SOFC for electricity and fresh water production. Energy Convers Manag. 2019;196:296–310. https://doi.org/10.1016/J.ENCONMAN.2019.06.006.

28. Behzadi A, Gholamian E, Houshfar E, Ashjaee M, Habibollahzade A. Thermoeconomic analysis of a hybrid PVT solar system integrated with double effect absorption chiller for cooling/hydrogen production. Energy Equip. Syst. 2018;6:413–27. https://doi.org/10.22059/ees.2018.33319.

29. Jokar MA, Ahmadi MH, Sharifpur M, Meyer JP, Pourfayaz F, Ming T. Thermodynamic evaluation and multi-objective optimization of molten carbonate fuel cell-supercritical CO2 Brayton cycle hybrid system. Energy Convers Manag. 2017;153:538–56. https://doi.org/10.1016/J.ENCONMAN.2017.10.027.

30. Safari F, Dincer I. Development and analysis of a novel biomass-based integrated system for multigeneration with hydrogen production. Int J Hydrogen Energy. 2019;44:3511–26. https://doi.org/10.1016/J.IJHYDENE.2018.12.101.

31. Beigzadeh M, Pourfayaz F, Ahmadi MH. Modeling and improvement of solid oxide fuel cell-single effect absorption chiller hybrid system by using nanofluids as heat transporters. Appl Therm Eng. 2020;166:114707. https://doi.org/10.1016/J.APPLTHERMALENG.2019.114707.

32. Behzadi A, Habibollahzade A, Ahmadi P, Gholamian E, Houshfar E. Multi-objective design optimization of a solar based system for electricity, cooling, and hydrogen production. Energy. 2019;169:696–709. https://doi.org/10.1016/J.ENERGY.2018.12.047.

33. Gholamian E, Zare V. A comparative thermodynamic investigation with environmental analysis of SOFC waste heat to power conversion employing Kalina and organic rankine cycles. Energy Convers Manag. 2016;117:150–61. https://doi.org/10.1016/j.enconman.2016.03.011.

34. Gholamian E, Zare V, Mousavi SM. Integration of biomass gasification with a solid oxide fuel cell in a combined cooling, heating and power system: a thermodynamic and environmental analysis. Int J Hydrogen Energy. 2016. https://doi.org/10.1016/j.ijhydene.2016.07.217.

35. Gholamian E, Hanafizadeh P, Ahmadi P, Mazzarella L. A transient optimization and techno-economic assessment of a building integrated combined cooling, heating and power system in Tehran. Energy Convers Manag. 2020;217:112962. https://doi.org/10.1016/J.ENCONMAN.2020.112962.

36. Behzadi A, Arabkoohsar A. Comparative performance assessment of a novel cogeneration solar-driven building energy system integrating with various district heating designs. Energy Convers Manag. 2020;220:113101. https://doi.org/10.1016/J.ENCONMAN.2020.113101.

37. Al-Khori K, Bicer Y, Koç M. Integration of solid oxide fuel cells into oil and gas operations: needs, opportunities, and challenges. J Clean Prod. 2020;245:118924. https://doi.org/10.1016/J.JCLEPRO.2019.118924.

38. Gholamian E, Hanafizadeh P, Ahmadi P. Exergo-economic analysis of a hybrid anode and cathode recycling SOFC/Stirling engine for aviation applications. Int. J. Sustain. Aviat. 2018;4:11. https://doi.org/10.1504/IJSA.2018.092915.

39. Yari M, Mehr AS, Mahmoudi SMS, Santarelli M. A comparative study of two SOFC based cogeneration systems fed by municipal solid waste by means of either the gasifier or digester. Energy. 2016;114:586–602. https://doi.org/10.1016/j.energy.2016.08.035.

40. Khani L, Mehr AS, Yari M, Mahmoudi SMS. Multi-objective optimization of an indirectly integrated solid oxide fuel cell-gas turbine cogeneration system. Int J Hydrogen Energy. 2016;41:21470–88. https://doi.org/10.1016/J.IJHYDENE.2016.09.023.

41. Eshraghi A, Salehi G, Heibati S, Lari K. An assessment of the effect of different energy storage technologies on solar power generators for different power sale scenarios: the case of Iran. Sustain. Energy Technol. Assessments. 2019;34:62–7. https://doi.org/10.1016/J.SETA.2019.04.006.

42. Sadaghiani MS, Ahmadi MH, Mehrpooya M, Pourfayaz F, Feidt M. Process development and thermodynamic analysis of a novel power generation plant driven by geothermal energy with liquefied natural gas as its heat sink. Appl Therm Eng. 2018;133:645–58. https://doi.org/10.1016/J.APPLTHERMALENG.2018.01.077.

43. Bejan A, Moran MJ. Thermal design and optimization. Hoboken: Wiley; 1996.

44. Wu C, Wang SS, Feng XJ, Li J. Energy, exergy and exergoeconomic analyses of a combined supercritical CO2 recompression Brayton/absorption refrigeration cycle. Energy Convers Manag. 2017;148:360–77. https://doi.org/10.1016/j.enconman.2017.05.042.

45. Balli O, Aras H, Hepbasli A. Thermodynamic and thermoeconomic analyses of a trigeneration (TRIGEN) system with a gas-diesel engine: part I—Methodology. Energy Convers Manag. 2010;51:2252–9. https://doi.org/10.1016/j.enconman.2010.03.021.

46. Indicators, Economic. "Marshall&Swift equipment cost index." Chem Eng 72 (2011).

47. Dinçer I, Rosen M, Ahmadi P. Optimization of energy systems. Hoboken: Wiley; 2017.

48. Rokni M. Thermodynamic and thermoeconomic analysis of a system with biomass gasification, solid oxide fuel cell (SOFC) and Stirling engine. Energy. 2014;76:19–31. https://doi.org/10.1016/j.energy.2014.01.106.

49. Sánchez D, Chacartegui R, Torres M, Sánchez T. Stirling based fuel cell hybrid systems: an alternative for molten carbonate fuel cells. J Power Sources. 2009;192:84–93. https://doi.org/10.1016/j.jpowsour.2008.12.061.

50. Assar M, Blumberg T, Morosuk T, Tsatsaronis G. Comparative exergoeconomic evaluation of two modern combined-cycle power plants. Energy Convers Manag. 2016;153:616–26. https://doi.org/10.1016/j.enconman.2017.10.036.

51. Habibollahzade A, Houshfar E, Ashjaee M, Gholamian E, Behzadi A. Enhanced performance and reduced payback period of a low grade geothermal-based ORC through employing two TEGs. Energy Equip. Syst. 2019;7:23–39. https://doi.org/10.22059/EES.2019.34611.

52. Landau L, Moran MJ, Shapiro HN, Boettner DD, Bailey M. Fundamentals of engineering thermodynamics. Hoboken: Wiley; 2010.

53. Gholamian E, Hanafizadeh P, Ahmadi P. Advanced exergy analysis of a carbon dioxide ammonia cascade refrigeration system. Appl. Therm. Eng. 2018;137:689–99. https://doi.org/10.1016/j.applthermaleng.2018.03.055.

54. Ahmadi P, Dincer I, Rosen MA. Exergy, exergoeconomic and environmental analyses and evolutionary algorithm based multi-objective optimization of combined cycle power plants. Energy. 2011;36:5886–98. https://doi.org/10.1016/J.ENERGY.2011.08.034.

55. S. Mohammad, S. Mahmoudi, E. Gholamian, V. Zare, Exergy analysis of a new configuration of trigeneration system based on biomass Gasifier, (n.d.). https://www.researchgate.net/profile/Ehsan_Gholamian/publication/311270911_EXERGY_ANALYSIS_OF_A_NEW_CONFIGURATION_OF_TRIGENERATION_SYSTEM_BASED_ON_BIOMASS_GASIFIER/links/58405cd108ae2d21755f3299.pdf (accessed June 27, 2017).

56. Behzadi A, Arabkoohsar A, Gholamian E. Multi-criteria optimization of a biomass-fired proton exchange membrane fuel cell integrated with organic rankine cycle/thermoelectric generator using different gasification agents. Energy. 2020;201:117640. https://doi.org/10.1016/J.ENERGY.2020.117640.

57. Holland JH. Adaptation in natural and artificial systems: an introductory analysis with applications to biology, control, and artificial intelligence. Ann Arbor: University of Michigan Press; 1975.

58. Tao G, Armstrong T, Virkar A, Intermediate temperature solid oxide fuel cell (IT-SOFC) research and development activities at MSRI. In: Ninet. Annu. ACERC&ICES Conf. Utah, 2005.

59. Hosseinpour J, Sadeghi M, Chitsaz A, Ranjbar F, Rosen MA. Exergy assessment and optimization of a cogeneration system based on a solid oxide fuel cell integrated with a stirling engine. Energy Convers Manag. 2017;143:448–58. https://doi.org/10.1016/J.ENCONMAN.2017.04.021.

60. Gomri R, Hakimi R. Second law analysis of double effect vapour absorption cooler system. Energy Convers Manag. 2008;49:3343–8.